J. Fluid Mech. (2005), *vol.* 525, *pp.* 37–72.
DOI: 10.1017/S0022112004002551 Printed in the United Kingdom

The role of instability waves in predicting jet noise

By M. E. GOLDSTEIN[1] AND S. J. LEIB[2]

[1]National Aeronautics and Space Administration, Glenn Research Center, Cleveland, OH 44135, USA
[2]Ohio Aerospace Institute, Brook Park, OH 44142, USA

(Received 3 May 2004 and in revised form 27 September 2004)

There is a continuing debate about the role of linear instability waves in the prediction of jet noise. Parallel mean flow models, such as the one proposed by Lilley, usually neglect these waves because they cause the solution to become infinite. The result is then non-causal and can, therefore, be quite different from the more realistic causal solution, especially for the chaotic flows being considered here. The present paper solves the relevant acoustic equations for a non-parallel mean flow by using a vector Green's function approach and requiring that the mean flow be weakly non-parallel, i.e. requiring that the spread rate be small. It demonstrates that linear instability waves must be accounted for in order to construct a proper causal solution to the jet noise problem. Recent experimental results (e.g. see Tam, Golebiowski & Seiner 1996) show that the small-angle spectra radiated by supersonic jets are significantly different from those radiated at larger angles (say, at 90°) and even exhibit dissimilar frequency scalings (i.e. they scale with Helmholtz number as opposed to Strouhal number). The present solution is (among other things) able to explain this rather puzzling experimental result.

1. Introduction

Lighthill (1952, 1954) provided a systematic basis for predicting jet noise when he rearranged the Navier–Stokes equations into the form of a linear wave equation for a medium at rest with a quadrupole-type source term (which includes a pressure/density contribution that Lilley (1974) showed to be more appropriately described by a dipole-type source.) The crucial step in this so-called acoustic analogy approach amounts to assuming that the source term is in some sense known or that it can at least be modelled in an approximate fashion. Early efforts to improve the Lighthill approach focused on accounting for mean flow interaction effects. Phillips (1960), Lilley (1974), and many others, sought to accomplish this by rearranging the Navier–Stokes equations into the form of an inhomogeneous convective, or moving-medium, wave equation rather than the inhomogeneous stationary-medium wave equation originally proposed by Lighthill. Current industrial noise prediction methods, such as GE's MGB approach (Balsa *et al.* 1978), are based on a form of the convective wave equation proposed by Lilley (1974) in which the wave operator is appropriate to sound propagation on a parallel mean flow and therefore possesses homogeneous solutions corresponding to spatially growing instability waves on that flow (Betchov & Criminale 1967).

The complete solution to this equation consists of a particular solution plus these homogeneous contributions, but the result cannot be used to calculate the far-field noise because the instability waves become unbounded (infinite) far downstream in the

flow. The usual resolution to this dilemma is to completely neglect the contribution of the instability waves. Unfortunately, the resulting solution turns out to be non-causal, which may be particularly serious in flows that support instabilities (i.e. chaotic flows) because small changes in initial (and/or boundary) conditions can produce large (i.e. $O(1)$) changes in the steady-state solution. Arguments against imposing a causality requirement (Mani 1976; Dowling, Ffowcs Williams & Goldstein 1978) usually amount to asserting that it is unnecessary because it is not possible to identify an initial time before which the fluctuations (about the base flow) have been 'switched on' in an acoustic analogy approach and that a boundedness requirement can, therefore, be imposed on the solution.

A better approach might be to begin with an equation appropriate to sound propagation on a non-parallel flow, say the actual mean flow in the jet. The most important difference between this approach and Lilley's parallel flow result is that the homogeneous solutions to the acoustic equations correspond to instability waves that grow and then decay on the diverging, non-parallel base flow and therefore always remain bounded – which eliminates the dilemma alluded to above. But since the homogeneous solutions are now bounded, this leaves the mathematical problem incompletely specified (i.e. ill posed) and the imposition of causality appears to be the most reasonable way of making the solution unique in this case. Our view is that the causality amounts to more than just imposing appropriate initial conditions and that it serves (as demonstrated at the end of § 4) to ensure the appropriate cause–effect relation between the sound and its turbulent source when it is imposed on the Green's function, as is done below.

The present paper develops a causal solution to the relevant acoustic equations by using a vector Green's function approach and assuming that the mean flow spread rate, say ε, is small. This implies that all streamwise changes in that flow occur on the slow streamwise length scale εx_1, where x_1 is the (suitably normalized) coordinate in the flow direction. The appropriate casual Green's function consists of a component that decays to zero when the unscaled streamwise coordinate $x_1 - x_1'$ becomes large (where x_1' corresponds to the source location) plus a component that becomes unbounded when the unscaled streamwise coordinate becomes large but decays to zero on the long (slow) streamwise length scale $\varepsilon\ (x_1 - x_1')$. The former component can be calculated by treating the slow variable εx_1 as a parameter and using the locally parallel flow approximation to simplify the results.

This approximation cannot, however, be used to determine the latter component (which corresponds to a superposition of linear instability waves; Briggs 1964; Bers 1975), since the resulting local solution would become unbounded and would not remain valid over the long streamwise length scale $\varepsilon\ (x_1 - x_1')$ on which this component evolves. The appropriate result is obtained by retaining $O(\varepsilon)$ terms in the Green's function equations and using the method of multiple scales, the WKBJ method and matched asymptotic expansions to render the solution uniformly valid.

Both components of the Green's function act on the same source term and each is capable of producing acoustic radiation – even at subsonic Mach numbers. The first corresponds to the usual Lilley equation solution, but with slowly varying coefficients and with slightly modified source terms. The second is associated with linear instability waves, but is very different from conventional instability models since these waves are now continuously 'generated' along the length of the jet and do not constitute separate sound sources. Their only role is to produce the appropriate Green's function, and they may not even correspond to actual physical flow structures. Mani's (1976) assertion that the instability waves generate the turbulence and should, therefore, be

excluded is irrelevant here because their inclusion in the Green's function only serves to produce the appropriate cause–effect relation between the sound and its turbulent source and, therefore, corresponds to a different aspect of their behaviour.

Each component of this function can be thought of as a filter that only allows certain elements of the source spectrum to reach the far field. The resulting acoustic spectrum is expected to exhibit a bi-modal structure because the second Green's function component only responds to frequencies in the range where the instabilities exhibit spatial growth, which is somewhat lower than the frequency range selected by the first term. Preliminary calculations for a two-dimensional mixing layer (Goldstein & Handler 2003) suggest that the contribution of the second Green's function component will be fairly small at subsonic Mach numbers, but that it should be quite large at supersonic speeds and dominate the first term at small angles to the downstream jet axis. Recent experimental results (e.g. see Tam, Golebiowski & Seiner 1996) show that the small-angle spectra radiated by supersonic jets are quite different from those radiated at larger angles (say, at 90°) and even exhibit dissimilar frequency scalings (i.e. they scale with Helmholtz number as opposed to Strouhal number). Until now this curious behaviour seems to have defied explanation, but our model calculations show that it can be attributed to the fact that each of these Green's function components is the dominant carrier of the acoustic radiation at different angles to the jet axis. As noted above, the large differences between the present result and the usual non-causal Lilley's equation solutions are directly related to the chaotic nature of the flow.

The fundamental acoustic equations, which we refer to as the LNS equations, are introduced in § 2 and Lilley's equation as well as the equations for a steady but non-parallel base flow (i.e. the actual time-average flow) are obtained as special cases in § 3. A formal vector Green's function solution to the general LNS equations is given in § 4 and a local causal small-ε asymptotic approximation to this solution is constructed in § 5. The corresponding uniformly valid solution is obtained in § 6, and its far-field expansion is worked out in § 7. This result is then used to derive an expression for the far-field acoustic spectrum in § 8. The general formulae are applied to a round jet in § 9 and some simplifying approximations are introduced in § 10. Section 11 contains some qualitative comparisons between the numerical computations based on this simplified model and the available experimental data.

2. The fundamental equations

The Navier–Stokes equations can be written as

$$\frac{\partial}{\partial t}\Lambda_\nu + \frac{\partial}{\partial x_j}\Gamma_{\nu j} = 0, \tag{2.1}$$

where the summation convention is being used, but with the Greek indices ranging from 1 to 5 (to represent the five first-order equations), while the Latin indices i, j are restricted to the range 1, 2, 3, $\{\Lambda_\nu\} = \{\rho v_i, \rho h_o - p, \rho\}$,

$$\{\Gamma_{\nu j}\} = \{\rho v_i v_j + \delta_{ij} p - \sigma_{ij},\ \rho v_j h_o + q_j - v_i \sigma_{ij},\ \rho v_j\}, \quad \text{where}$$
$$h_o \equiv h + \tfrac{1}{2}v^2 \tag{2.2}$$

denotes the stagnation enthalpy, h denotes the enthalpy, t denotes the time, $\boldsymbol{x} \equiv \{x_1, x_2, x_3\}$ are Cartesian coordinates, p denotes the pressure, ρ denotes the density, $\boldsymbol{v} = \{v_1, v_2, v_3\}$ is the fluid velocity, σ_{ij} is the viscous stress tensor, q_i is the heat flux vector, and $\{\rho v_i, \rho h_o - p, \rho\}$ is shorthand for $\{\rho v_1, \rho v_2, \rho v_3, \rho h_o - p, \rho\}$ etc. The

dependent variables are assumed to satisfy the ideal gas law:

$$p = \rho RT, \quad h = c_p T, \tag{2.3}$$

with $R = c_p - c_v$ being the gas constant, c_p and c_v are the specific heats at constant pressure and volume, respectively, and T the absolute temperature. Goldstein (2002) showed that (2.1) can be recast into the form of the linearized Navier–Stokes equations by dividing the dependent variables

$$\rho = \bar{\rho} + \rho', \quad p = \bar{p} + p', \quad h = \tilde{h} + h', \quad v_i = \tilde{v}_i + v_i', \tag{2.4}$$

as well as the viscous stress σ_{ij} and heat flux q_i, into their 'base flow' components $\bar{\rho}, \bar{p}, \tilde{h}, \tilde{v}_i, \bar{\sigma}_{ij}$, and $\bar{q}_i$, and their 'residual' components $\rho', p', h', v_i', \sigma_{ij}'$, and q_i', and requiring that the former satisfy the inhomogeneous Navier–Stokes equations

$$\frac{\partial}{\partial t}\tilde{\Lambda}_v + \frac{\partial}{\partial x_j}\tilde{\Gamma}_{vj} = 0, \tag{2.5}$$

along with an ideal gas law equation of state,

$$\tilde{h} = c_p \tilde{T} = \frac{c_p}{R}\frac{\bar{p}}{\bar{\rho}}, \tag{2.6}$$

where

$$\left.\begin{aligned} &\{\tilde{\Lambda}_v\} = \{\bar{\rho}\tilde{v}_i,\ \bar{\rho}\tilde{h}_o - \bar{p} - \tilde{H}_o,\ \bar{\rho}\},\\ &\{\tilde{\Gamma}_{vj}\} = \{\bar{\rho}\tilde{v}_i\tilde{v}_j + \delta_{ij}\bar{p} - \bar{\sigma}_{ij} - \tilde{T}_{ij},\ \bar{\rho}\tilde{v}_j\tilde{h}_o + \bar{q}_j - \tilde{v}_i\bar{\sigma}_{ij} - \tilde{H}_j - \tilde{v}_j\tilde{H}_o,\ \bar{\rho}\tilde{v}_j\},\\ &\tilde{h}_o \equiv \tilde{h} + \tfrac{1}{2}\tilde{v}^2 \end{aligned}\right\} \tag{2.7}$$

is the base flow stagnation enthalpy, and the 'source strengths' $\tilde{T}_{ij}$, $\tilde{H}_o$, and $\tilde{H}_j$, which are assumed to be localized, can otherwise be specified arbitrarily.

The residual variables are governed by the linearized Navier–Stokes (LNS) equations

$$L_{\mu v} u_v = s_\mu, \tag{2.8}$$

where

$$\{u_v\} \equiv \{\bar{\rho}u_i',\ p_o',\ \rho'\}, \tag{2.9}$$

with

$$\bar{\rho}u_i' \equiv \rho v_i' \tag{2.10}$$

and

$$p_o' \equiv p' + (\gamma - 1)\left(\tfrac{1}{2}\rho v'^2 + \tilde{H}_o\right), \tag{2.11}$$

is a five-dimensional (nonlinear) dependent variable vector,

$$L_{\mu v} \equiv \delta_{\mu v}\mathrm{D}_o + \delta_{v4}\partial_\mu + \partial_v(\widetilde{c^2}\delta_{\mu 4} + \delta_{\mu 5}) + K_{\mu v}, \tag{2.12}$$

with

$$K_{\mu v} \equiv \partial_v\tilde{v}_\mu - \frac{1}{\bar{\rho}}\frac{\partial\tilde{\tau}_{\mu j}}{\partial x_j}\delta_{v5} + (\gamma - 1)\left(\frac{\partial\tilde{v}_j}{\partial x_j}\delta_{v4} - \frac{1}{\bar{\rho}}\frac{\partial\tilde{\tau}_{vj}}{\partial x_j}\right)\delta_{\mu 4}, \tag{2.13}$$

$$\tilde{\tau}_{ij} \equiv \delta_{ij}\bar{p} - \tilde{T}_{ij} - \bar{\sigma}_{ij}, \tag{2.14}$$

$$\partial_\mu \equiv \frac{\partial}{\partial x_i}, i = \mu = 1, 2, 3, \tag{2.15}$$

is the five-dimensional linear Euler operator. D_o denotes the linear operator

$$\mathrm{D}_o \equiv \frac{\partial}{\partial t} + \frac{\partial}{\partial x_j}\tilde{v}_j, \tag{2.16}$$

and $\partial_\mu, \tilde{v}_\mu, \tilde{\tau}_{\mu j}$ are all equal to zero when $\mu > 3$. The five-dimensional source vector s_μ is given by

$$s_\mu \equiv \frac{\partial}{\partial x_j} e'_{j\mu} + \delta_{\mu 4}(\gamma - 1) e'_{ij} \frac{\partial \tilde{v}_i}{\partial x_j}, \tag{2.17}$$

where $\gamma \equiv c_p/c_v$ is the specific heat ratio, the source strengths e'_{iv} are given by

$$e'_{iv} \equiv -\rho v'_i v'_v - \tilde{T}_{iv} + \delta_{iv}(\gamma - 1)\left(\frac{\rho v'^2}{2} + \tilde{H}_o\right) + \sigma'_{iv}, \tag{2.18}$$

for $v = 1, 2.., 4$ and zero otherwise and we have put

$$v'_4 \equiv (\gamma - 1)\left(h' + \tfrac{1}{2}v'^2\right) = c^{2'} + \frac{(\gamma - 1)}{2}v'^2, \tag{2.19}$$

$$\tilde{T}_{i4} = (\gamma - 1)(\tilde{H}_i - \tilde{T}_{ij}\tilde{v}_j) \tag{2.20}$$

and

$$\sigma'_{j4} = -(\gamma - 1)(q'_j - \sigma_{jl}v'_l). \tag{2.21}$$

Equation (2.8) is easily converted into the usual convective form of the LNS equations by using the fifth component of the base flow equation (2.5) to show that

$$\mathrm{D}_o \bar{\rho} f = \bar{\rho}\left(\frac{\partial}{\partial t} + \tilde{v}_j \frac{\partial}{\partial x_j}\right) f. \tag{2.22}$$

They are written out in the more familiar, but less compact, vector form in Goldstein (2002).

3. Lilley's equation and the non-parallel mean flow result

The base flow equation (2.5) reduces to the usual Euler equations when the arbitrary source strengths $\tilde{T}_{ij}$, $\tilde{H}_j$, and $\tilde{H}_o$, and the mean viscous stress $\bar{\sigma}_{ij}$ and heat flux $\bar{q}_i$ are set equal to zero. A general class of solutions to these equations, which quite conveniently provides a good approximation to the mean flow field in a real jet, is the *unidirectional transversely sheared mean flow*

$$\tilde{v}_i = \delta_{i1}U(x_2, x_3), \quad \bar{p} = \text{constant}, \quad \bar{\rho} = \bar{\rho}(x_2, x_3). \tag{3.1}$$

The fifth component of the LNS equation then decouples from the remaining four components, which now become the inhomogeneous compressible Rayleigh equations (Betchov & Criminale 1967)

$$\bar{\rho}\left(\frac{\mathrm{D}_o u'_i}{\mathrm{D}t} + \delta_{i1}u'_j \frac{\partial U}{\partial x_j}\right) + \frac{\partial p'_o}{\partial x_i} = \frac{\partial}{\partial x_j}e'_{ij}, \tag{3.2}$$

$$\frac{\mathrm{D}_o p'_o}{\mathrm{D}t} + \gamma \bar{p}\frac{\partial u'_j}{\partial x_j} = \frac{\partial e'_{4j}}{\partial x_j} + (\gamma - 1)e'_{1j}\frac{\partial U}{\partial x_j}, \tag{3.3}$$

where D_o reduces to the usual convective derivative

$$\mathrm{D}_o = \frac{\mathrm{D}_o}{\mathrm{D}t} \equiv \frac{\partial}{\partial t} + U\frac{\partial}{\partial x_1}. \tag{3.4}$$

It is now well known (Goldstein 1976, chapter 1), that the velocity-like variable u_i' can be eliminated between these equations (by taking the divergence of the first equation and the convective derivative of the second, subtracting the results and then using the first equation to eliminate the velocity fluctuation on the left-hand side) to obtain the inhomogeneous Pridmore-Brown (1958) equation

$$\mathrm{L}p_o' = \frac{\mathrm{D}_o}{\mathrm{D}t}\left(\frac{\partial}{\partial x_i}\widetilde{c^2}\frac{\partial e_{ij}'}{\partial x_j}\right) - \frac{\partial U}{\partial x_i}2\widetilde{c^2}\frac{\partial^2 e_{ij}'}{\partial x_1 \partial x_j} - \frac{\mathrm{D}_o^2}{\mathrm{D}t^2}\left[\frac{\partial e_{4j}'}{\partial x_j} + (\gamma-1)e_{1j}'\frac{\partial U}{\partial x_j}\right] \tag{3.5}$$

where

$$\mathrm{L} \equiv \frac{\mathrm{D}_o}{\mathrm{D}t}\left(\frac{\partial}{\partial x_i}\widetilde{c^2}\frac{\partial}{\partial x_i} - \frac{\mathrm{D}_o^2}{\mathrm{D}t^2}\right) - 2\frac{\partial U}{\partial x_j}\frac{\partial}{\partial x_1}\widetilde{c^2}\frac{\partial}{\partial x_j} \tag{3.6}$$

is the variable-density Pridmore-Brown (1958) operator, and

$$\widetilde{c^2} = \gamma\bar{p}/\bar{\rho}(x_2, x_3) \tag{3.7}$$

is the square of the mean flow sound speed.

This is a form of Lilley's equation that was derived in Goldstein (2002). As noted in the Introduction, it possesses homogeneous solutions corresponding to spatially growing instability waves on the base flow (3.1) (Betchov & Criminale 1967). It also possesses homogeneous solutions corresponding to the continuous spectrum. The complete solution to this equation consists of a particular solution plus these homogeneous contributions, but the result is meaningless because the instability waves become unbounded (infinite) far downstream in the flow. The usual resolution to this dilemma is to completely neglect the instability wave contribution. Unfortunately, this causes the solution to be non-causal which, as noted in the Introduction, can lead to erroneous results.

A better resolution is obtained by choosing the base flow in (2.8) to be the actual mean flow of the jet. The overbars on the dependent base flow variables then denote the time average

$$\bar{\bullet} \equiv \lim_{T\to\infty}\frac{1}{2T}\int_{-T}^{T}\bullet(\boldsymbol{x}, t)\,\mathrm{d}t \tag{3.8}$$

where the dot stands for ρ, v_i, p, and h, and

$$\tilde{\bullet} \equiv (\overline{\rho\bullet}/\bar{\rho}) \tag{3.9}$$

denotes a Favre (1969) averaged quantity for all variables except $\tilde{h}_o$, which is defined by (2.7). Notice that (2.6) is completely consistent with the overall ideal gas law (2.3) when the tilde is defined in this fashion.

The time derivatives drop out of the base flow equations (2.5) and the source strengths are given by

$$\tilde{T}_{iv} = -\bar{\rho}\widetilde{v_i'v_v'}, \tag{3.10}$$

$$\tilde{H}_o = \tfrac{1}{2}\tilde{T}_{ii}. \tag{3.11}$$

The base flow equations are now the ordinary Reynolds-averaged Navier–Stokes (RANS) equations, which do not, of course, form a closed system. They are usually closed by assuming some sort of model relating the source terms to the mean flow variables $\tilde{v}_i$, $\bar{\rho}$, $\bar{p}$, and $\tilde{h}$ and their derivatives, such as a Boussinesq model (Speziale 1991; Speziale & So 1998) for the Reynolds stresses and a similar model for $\tilde{H}_j$.

The most important difference between these results and the parallel flow result is that the homogeneous solutions to the LNS equations, which now correspond to

instability waves growing and then decaying on the diverging non-parallel base flow, will always remain bounded. This eliminates the paradox alluded to above and the corresponding LNS equations can be used to calculate the radiated sound. The exact solution for a jet emanating from a nozzle consists of a particular solution that is driven by the sources (i.e. it satisfies causality and therefore the appropriate initial and far-field boundary conditions) and a homogeneous solution that is determined by the details of the nozzle geometry. The latter solution, which would be expected to vary considerably with experimental conditions and, therefore, be of only limited value as a predictive tool, is also somewhat inconsistent in that the instability waves must eventually become nonlinear in the actual flow while being forced to remain linear in the acoustic analogy framework. This solution has already been considered by Tam & Morris (1980), Tam & Burton (1984) and others and only appears to be important at high supersonic Mach numbers and/or for jets at high temperature ratios (Mani 1976; Tam 1995) where Mach wave radiation becomes dominant. We therefore restrict our attention to relatively low Mach number supersonic flows (say, $M \leqslant 1.6$) and consider the former solution, which can be written in terms of the *causal* vector Green's function for these equations. The general result for an arbitrary base flow is given in the next section.

4. Formal Green's function solution for the LNS equations

The particular solution can, as noted above, be expressed in terms of the vector Green's function (Morse & Feshbach 1953, pp. 878–886) $g_{v\sigma}(\boldsymbol{x}, t|\boldsymbol{x}', t')$, which satisfies

$$\mathrm{L}_{\mu v}\, g_{v\sigma} = \delta_{\mu\sigma}\delta(\boldsymbol{x}-\boldsymbol{x}')\delta(t-t'), \tag{4.1}$$

together with the causality condition

$$g_{v\sigma}(\boldsymbol{x}, t|\boldsymbol{x}', t') = 0 \quad \text{for} \quad t < t', \tag{4.2}$$

and leads to the following formula for the dependent variable vector u_v:

$$u_v(\boldsymbol{x}, t) = \int_{-\infty}^{\infty}\int_V g_{v\mu}(\boldsymbol{x}, t|\boldsymbol{x}', t')s_\mu(\boldsymbol{x}', t')\,\mathrm{d}\boldsymbol{x}'\,\mathrm{d}t', \tag{4.3}$$

where the symbol V denotes integration over all space.

The derivatives acting on the source strengths $e'_{j\mu}$in (2.17) can be transferred to the Green's function to obtain

$$u_v(\boldsymbol{x}, t) = -\int_{-\infty}^{\infty}\int_V \tilde{\gamma}_{vj\mu}e'_{\mu j}\,\mathrm{d}\boldsymbol{x}'\,\mathrm{d}t', \tag{4.4}$$

where

$$\tilde{\gamma}_{vj\mu}(\boldsymbol{x}, t|\boldsymbol{x}', t') \equiv \frac{\partial}{\partial x'_j}g_{v\mu} - (\gamma-1)\frac{\partial\tilde{v}_\mu}{\partial x'_j}g_{v4}. \tag{4.5}$$

From the acoustics perspective, the primary interest is in the fourth (i.e. the pressure-like) component of (4.3), which, in view of (2.14), (2.18) to (2.21), (3.10) and (3.11) can be written as

$$p'_o = \int_{-\infty}^{\infty}\int_V \gamma_{j\mu}(\boldsymbol{x}, t|\boldsymbol{x}', t')\tau_{\mu j}(\boldsymbol{x}', t')\,\mathrm{d}\boldsymbol{x}'\,\mathrm{d}t' \tag{4.6}$$

where

$$\gamma_{j\mu} \equiv -\frac{\partial}{\partial x'_j}g_{4\mu} + \frac{\gamma-1}{2}\delta_{j\mu}\frac{\partial g_{4l}}{\partial x'_l} + (\gamma-1)\left(\frac{\partial\tilde{v}_\mu}{\partial x'_j} - \frac{\gamma-1}{2}\delta_{j\mu}\frac{\partial\tilde{v}_l}{\partial x'_l}\right)g_{44} \tag{4.7}$$

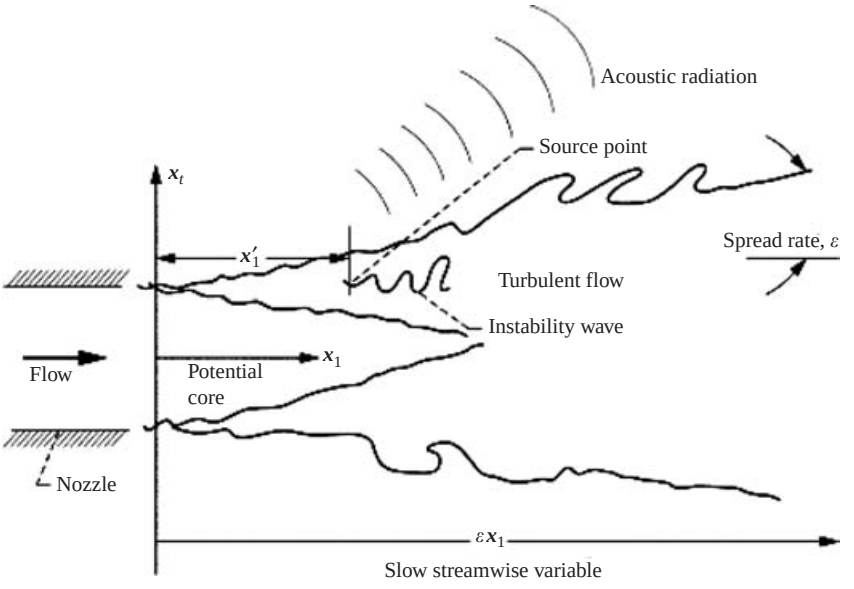

FIGURE 1. Turbulent jet flow field.

and

$$\tau_{\mu j} \equiv -(\rho v_j' v_\mu' - \bar{\rho}\,\widetilde{v_j' v_\mu'}) + \sigma_{j\mu}', \tag{4.8}$$

when the bulk viscosity is zero and the base flow is taken to be the actual mean flow in the jet. So in the inviscid limit, which is of primary interest here, $\tau_{\mu j}$ is just a generalized four-dimensional fluctuating Reynolds stress and equation (4.6) therefore provides a direct linear relation between this quantity and the far-field pressure fluctuation (recall that p_o' reduces to the latter in the far field). Notice that the causality condition (4.2), which requires that the Green's function vanish when t is less than the emission time $t'$and does not depend on there being some initial time before all the fluctuations are 'switched on', merely serves to ensure that all of the sound is generated by $\tau_{\mu j}$ and that none of it comes from extraneous sources.

5. The local Green's function solution for a slowly diverging mean flow

The exact solution to (4.1) would require extensive numerical computation. But it is reasonable to seek an (approximate) asymptotic solution in the limit of small jet spread rate, say ε, since most jet flows are nearly parallel – especially those of technological interest (see figure 1). In this section, we obtain an appropriate local approximation for this result. To this end, we suppose that all lengths have been normalized by some characteristic cross-flow dimension of the jet (say its diameter, in the case of a round jet) and all velocities by some appropriate characteristic streamwise velocity with similar obvious normalization for the density, pressure and temperature. Then the mean flow velocities should expand like

$$\tilde{v}_1 = U(X, \boldsymbol{x}_\perp) + \varepsilon U^{(1)}(X, \boldsymbol{x}_\perp) + \ldots, \tag{5.1}$$

$$\tilde{\boldsymbol{v}}_\perp = \varepsilon \boldsymbol{V}(X, \boldsymbol{x}_\perp) + \varepsilon^2 \boldsymbol{V}^{(1)}(X, \boldsymbol{x}_\perp) + \ldots, \tag{5.2}$$

where

$$X \equiv \varepsilon\, x_1 \tag{5.3}$$

denotes the slow streamwise variable and

$$\boldsymbol{x}_\perp = \{x_2, x_3\}, \quad \tilde{\boldsymbol{v}}_\perp = \{\tilde{v}_2, \tilde{v}_3\} \tag{5.4}$$

denote cross-flow variables. The expansions for the remaining mean flow variables are given in Appendix A, where it is shown that the mean flow is determined (at lowest order) by (A 7) to (A 12) in the inviscid limit where $\bar{\sigma}_{ij} = \bar{q}_j = 0$ – which is clearly appropriate here, because the mean Reynolds stresses are much larger than the viscous stresses in most cases.

These results imply that the vector Green's function $g_{v\sigma}$ and the linear operator $\mathrm{L}_{\mu v}$ in (4.1) must expand like

$$g_{v\sigma}(\boldsymbol{x}, X, t|\boldsymbol{x}', X', t') = g^{(0)}_{v\sigma} + \varepsilon g^{(1)}_{v\sigma} + \ldots \tag{5.5}$$

and

$$\mathrm{L}_{\mu v} = \mathrm{L}^{(0)}_{\mu v} + \varepsilon \mathrm{L}^{(1)}_{\mu v} + \ldots . \tag{5.6}$$

Substituting (5.5) and (5.6), along with the mean flow variable expansions, into (4.1) shows that $g^{(0)}_{v\sigma}$ is determined by

$$\mathrm{L}^{(0)}_{iv} g^{(0)}_{v\sigma} \equiv \frac{\mathrm{D}_o}{\mathrm{D}t} g^{(0)}_{i\sigma} + \frac{\partial}{\partial x_i} g^{(0)}_{4\sigma} + \delta_{i1} \frac{\partial U}{\partial x_j} g^{(0)}_{j\sigma} = \delta_{i\sigma} \delta(\boldsymbol{x} - \boldsymbol{x}') \delta(t - t'), \tag{5.7a}$$

$$\mathrm{L}^{(0)}_{4v} g^{(0)}_{v\sigma} \equiv \frac{\mathrm{D}_o}{\mathrm{D}t} g^{(0)}_{4\sigma} + \frac{\partial}{\partial x_j} \left(\widetilde{c_0^2} g^{(0)}_{j\sigma} \right) = \delta_{4\sigma} \delta(\boldsymbol{x} - \boldsymbol{x}') \delta(t - t'), \tag{5.7b}$$

$$\mathrm{L}^{(0)}_{5v} g^{(0)}_{v\sigma} \equiv \frac{\mathrm{D}_o}{\mathrm{D}t} g^{(0)}_{5\sigma} + \frac{\partial}{\partial x_j} g^{(0)}_{j\sigma} = 0, \tag{5.7c}$$

for $\sigma = 1, \ldots 4$, where $\widetilde{c_0^2} = P/\bar{R}$, with P and $\bar{R}$ defined in (A1) and (A2), and $\mathrm{D}_o/\mathrm{D}t$ is given by equation (3.4). The first-order perturbations are given in Appendix B.

We begin by constructing a local solution that is valid in the vicinity of $x_1 = x_1'$, but, as indicated in the introduction, does not remain valid on the long streamwise length scale $X - X' = X - \varepsilon x_1'$ and can therefore not be used in (4.6) to calculate the distant sound field. This solution is corrected in the next subsection to obtain a uniformly valid result that overcomes this difficulty.

The left-hand sides of equations (5.7*a*, *b*) are essentially the same as those of the parallel flow equations (3.2) and (3.3) and the velocity-like variables can again be eliminated to obtain the following single equation for $g^{(0)}_{4\sigma}$:

$$\begin{aligned} \mathrm{L} g^{(0)}_{4\sigma} = {} & \frac{\mathrm{D}_o}{\mathrm{D}t} \frac{\partial}{\partial x_i} \widetilde{c_0^2} \delta_{i\sigma} \delta(\boldsymbol{x} - \boldsymbol{x}') \delta(t - t') \\ & - 2 \frac{\partial U}{\partial x_i} \widetilde{c_0^2} \frac{\partial}{\partial x_1} \delta_{i\sigma} \delta(\boldsymbol{x} - \boldsymbol{x}') \delta(t - t') - (\gamma - 1) \frac{\mathrm{D}_o^2}{\mathrm{D}t^2} \delta_{4\sigma} \delta(\boldsymbol{x} - \boldsymbol{x}') \delta(t - t'), \end{aligned} \tag{5.8}$$

where L is given by equation (3.6), but with $\widetilde{c^2}$ replaced by $\widetilde{c_0^2}$.

Since the coefficients in these equations are independent of time and only depend on x_1 through the slow variable X, a local (*causal*) solution can be obtained in the usual way by taking the double Fourier–Laplace transform

$$g^{(n)}_{v\sigma} = \int_{\mathrm{i}c-\infty}^{\mathrm{i}c+\infty} \int_{-\infty}^{\infty} \mathrm{e}^{\mathrm{i}[k(x_1 - x_1') - \omega(t - t')]} \bar{G}^{(n)}_{v\sigma}(\omega, k, X; \boldsymbol{x}_\perp | \boldsymbol{x}_\perp') \, \mathrm{d}k \, \mathrm{d}\omega \quad \text{for} \quad n = 0, 1, \tag{5.9}$$

where causality is enforced by requiring that the ω integration be over the Bromowitz contour, i.e. the contour (shown in figure 2) that lies above all the

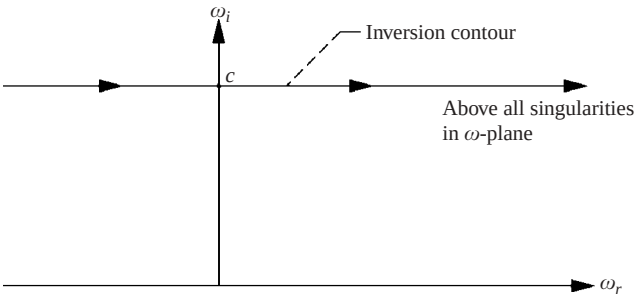

FIGURE 2. Laplace inversion contour.

singularities of $\bar{G}^{(0)}_{\nu\sigma}$. Appendix E shows that the fourth component Fourier–Laplace transform, $\bar{G}^{(0)}_{4\sigma}$, can be expressed in terms of a single *symmetric* function $\bar{G}_o(\omega, k, X; \boldsymbol{x}_\perp|\boldsymbol{x}'_\perp) = \bar{G}_o(\omega, k, X; \boldsymbol{x}'_\perp|\boldsymbol{x}_\perp)$ that satisfies

$$\mathscr{L}_k \bar{G}_o = \frac{\delta(\boldsymbol{x}_\perp - \boldsymbol{x}'_\perp)}{(2\pi)^2} \tag{5.10}$$

where $\mathscr{L}_k$ denotes the Rayleigh operator

$$\mathscr{L}_k \equiv \frac{\partial}{\partial x_j}\frac{\widetilde{c_0^2}}{(kU-\omega)^2}\frac{\partial}{\partial x_j} + 1 - \frac{k^2\widetilde{c_0^2}}{(kU-\omega)^2}, \quad j = 2, 3. \tag{5.11}$$

It, therefore, follows from (E3) that the fourth component of the lowest-order Green's function becomes

$$g^{(0)}_{4\sigma} = -\int_{\mathrm{i}c-\infty}^{\mathrm{i}c+\infty}\int_{-\infty}^{\infty}\frac{\widetilde{c_0^2}(\boldsymbol{x}'_\perp)}{[kU(\boldsymbol{x}'_\perp)-\omega]^2}\mathrm{D}'_\sigma\, \mathrm{e}^{\mathrm{i}[k(x_1-x'_1)-\omega(t-t')]}\bar{G}_0(\boldsymbol{x}_\perp|\boldsymbol{x}'_\perp)\,\mathrm{d}k\,\mathrm{d}\omega, \tag{5.12}$$

where

$$\mathrm{D}'_\sigma \equiv \begin{cases} \dfrac{\partial}{\partial x'_j} & \text{for } \sigma = j = 1, 2, 3 \\ \dfrac{-(\gamma-1)}{\widetilde{c_0^2}(\boldsymbol{x}'_\perp)}\left[\mathrm{i}\omega + U(\boldsymbol{x}'_\perp)\dfrac{\partial}{\partial x'_1}\right] & \text{for } \sigma = 4. \end{cases} \tag{5.13}$$

Steady-state solutions can only exist if the Laplace inversion contour can be continuously deformed onto the real axis (otherwise $\int_{-\infty}^{\infty}\exp(\mathrm{i}k(\boldsymbol{x}_1 - \boldsymbol{x}'_1))\bar{G}^{(0)}_{4\sigma}\,\mathrm{d}k$ would possess singularities in the upper half ω-plane, which would cause $g^{(0)}_{4\sigma}$ to grow without bound as $t \to \infty$ with $\boldsymbol{x}$ fixed). But jet flows are usually inviscibly unstable which means that $\bar{G}_0$ must possess (usually simple) poles in the upper half-k-plane that cross the real k-axis during this deformation. The k-integration contour c_k must obviously be deformed to lie below these poles (as shown in figure 3) in order to obtain a continuous result in the ω-plane (Briggs 1964; Bers 1975).

The poles correspond to the infinitely many discrete eigenvalues, say $k = \kappa_n(\omega, X)$, of the two-dimensional Rayleigh operator (5.11), but only a finite number of them cross into the lower half-plane (since there are only a finite number of unstable modes; Wundrow 1996) when the cross-section of the jet is finite. The integral over c_k can then be decomposed into an integral over the real k-axis plus a finite number

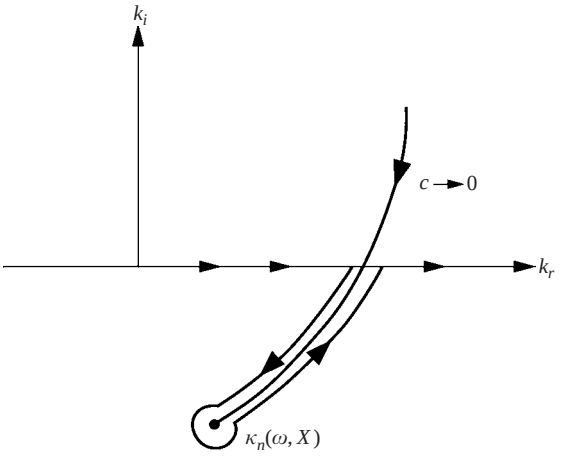

FIGURE 3. Fourier inversion contour.

of contour integrals which can be evaluated as the sum of the residues of the poles that have crossed the real axis.

Assuming simple poles, $\bar{G}_o$ must behave like

$$\bar{G}_o \sim \frac{\Gamma_n(\boldsymbol{x}_\perp|\boldsymbol{x}'_\perp, \omega, X')}{k-\kappa_n} \quad \text{as } k \to \kappa_n \tag{5.14}$$

where Γ_n is bounded at $k=\kappa_n$. Substituting this into (5.10), multiplying by an arbitrary function $f(\boldsymbol{x}_\perp)$ and integrating over all $\boldsymbol{x}_\perp$ shows that

$$\int f(\boldsymbol{x}_\perp)\mathscr{L}_{\kappa_n}\Gamma_n \,\mathrm{d}\boldsymbol{x}_\perp = \frac{(k-\kappa_n)}{(2\pi)^2} f(\boldsymbol{x}'_\perp) \to 0 \quad \text{as } k \to \kappa_n. \tag{5.15}$$

But since f is arbitrary, this implies that $\mathscr{L}_{\kappa_n}\Gamma_n = 0$ and therefore that $\Gamma_n = \bar{\Gamma}_n(\boldsymbol{x}'_\perp, \omega, X')\varphi_n(\boldsymbol{x}_\perp)$, where φ_n is an eigenfunction corresponding to the eigenvalue κ_n. The corresponding spectrum may be degenerate with more than one eigenfunction corresponding to any given κ_n. It then follows from the symmetry property of $\bar{G}_o$ that Γ_n must be of the form

$$\Gamma_n = \frac{a_{lj}\varphi_{nl}(\boldsymbol{x}'_\perp)\varphi_{nj}(\boldsymbol{x}_\perp)}{\Delta'_n(\omega, X')} \quad \text{(no sum on } n\text{)} \tag{5.16}$$

where Δ'_n and $a_{lj} = a_{jl}$ are only determined when equation (5.10) is solved for $\bar{G}_o$.

The causal Green's function (5.12) can therefore be written as

$$\begin{aligned} g_{4\sigma}^{(0)} = &-\int_{-\infty}^{\infty}\int_{-\infty}^{\infty} \frac{\tilde{c_o^2}(\boldsymbol{x}'_\perp)}{[kU(\boldsymbol{x}'_\perp)-\omega]^2} \mathrm{D}'_\sigma \, \mathrm{e}^{\mathrm{i}[k(x_1-x'_1)-\omega(t-t')]} \bar{G}_0(\boldsymbol{x}_\perp|\boldsymbol{x}'_\perp)\,\mathrm{d}\omega\,\mathrm{d}k \\ &-2\pi\mathrm{i}\sum_n \int_{-\infty}^{\infty} \frac{\tilde{c_o^2}(\boldsymbol{x}'_\perp)a_{lj}\varphi_{nl}(\boldsymbol{x}_\perp)}{[\kappa_n U(\boldsymbol{x}'_\perp)-\omega]^2\Delta'_n} \mathrm{D}'_\sigma \, \mathrm{e}^{\mathrm{i}[\kappa_n(\omega,X)(x_1-x'_1)-\omega(t-t')]}\varphi_{nj}(\boldsymbol{x}'_\perp)\,\mathrm{d}\omega, \end{aligned} \tag{5.17}$$

where the sum is over the finite set of eigenvalues (which may be empty, i.e. the sum may be zero) that cross the real k-axis as the Laplace inversion contour approaches the real ω-axis.

6. The uniformly valid Green's function

The solution (5.17) consists of the sum of two terms, the first of which remains bounded, is a uniformly valid approximation to the true, non-parallel, result, and corresponds to the usual Lilley's equation solutions that appear in the literature. But the second term grows without bound as $x_1 - x_1'$ becomes large (since Im $\kappa_n < 0$) and therefore becomes invalid on the long streamwise length scale $X - X'$. We now show that more or less standard perturbation methods are used seriatim to render this term and, therefore, the entire Green's function (5.17) uniformly valid everywhere in the flow.

It can be made uniformly valid in the region $\boldsymbol{x}_\perp - \boldsymbol{x}_\perp' = 0(1)$, $X - X' = 0(1)$ occupied by the jet by using the method of multiple scales (see, for example, Crighton & Gaster 1976) to obtain

$$\text{2nd term in (5.17)} \;\rightarrow -2\pi\mathrm{i}\sum_n \int_{-\infty}^{\infty} \frac{\widetilde{c_o^2}(\boldsymbol{x}_\perp')A_{nl}(X|X')\varphi_{nl}(\boldsymbol{x}_\perp)a_{lj}}{[\kappa_n U(\boldsymbol{x}_\perp') - \omega]^2 \Delta_n'(\omega, X')} \times \mathrm{D}_\sigma' \exp\left(\mathrm{i}\left[\frac{1}{\varepsilon}\int_{X'}^{X} \kappa_n(\omega, X)\,\mathrm{d}X - \omega(t - t')\right]\right)\varphi_{nj}(\boldsymbol{x}_\perp')\,\mathrm{d}\omega, \quad (6.1)$$

where all quantities are evaluated at X', except where indicated and the amplitude function A_{nl} satisfies the initial condition

$$A_{nl}(X|X') \rightarrow 1 \qquad \text{as } X \rightarrow X' \quad (6.2)$$

but is otherwise determined by imposing a solvability requirement on the first-order solution $g_{v\sigma}^{(1)}$ which, as shown in Appendix C, implies that

$$h_{nl}^{(0)}\frac{\partial A_{nl}}{\partial X} + h_{nl}^{(1)}A_{nl} = 0 \quad (\text{no sum on } n, l), \quad (6.3)$$

where $h_{nl}^{(0)}$ and $h_{nl}^{(1)}$ are given by equations (C 9) to (C 14). The solution to equation (6.3) that satisfies (6.2) is

$$A_{nl} = \exp\left(-\int_{X'}^{X} h_{nl}(X)\,\mathrm{d}X\right) \quad (6.4)$$

where

$$h_{nl} \equiv h_{nl}^{(1)}/h_{nl}^{(0)}. \quad (6.5)$$

While (6.1) provides a uniformly valid approximation to the second $g_{4\sigma}^{(0)}$ term within the jet, the result is still not valid at large transverse distances because the solution $\varphi_{nl}^{(1)}$ of (C 3), which is a generalization of the second-order mode shape equation in the linear instability wave problem considered by Tam & Burton (1984), decays more slowly with $|\boldsymbol{x}_\perp|$ as $|\boldsymbol{x}_\perp| \rightarrow \infty$ than the first-order solution φ_{4nl} (see also Tam & Morris 1980). Tam & Burton consider only a round jet, but the large-$|\boldsymbol{x}_\perp|$ asymptotic behaviour of the present, more general, result is the same and their demonstration applies to the current situation as well. They also obtain an appropriate outer solution that remains valid at large transverse distances by using a Fourier transform approach, but we adopt a somewhat different approach, based on the WKBJ solution, to the reduced wave equation in order to deal with the more general (non-axisymmetric) flow being considered herein.

To this end we need only consider the factor

$$J_I \equiv A_{nl}(X|X')\exp\left(\frac{i}{\varepsilon}\int_{X'}^{X}\kappa_n(\omega, X)\,\mathrm{d}X\right)\varphi_{nl}(\boldsymbol{x}_\perp) \tag{6.6}$$

in (6.1). Once its far-field expansion is known, the result can be substituted back into this formula to obtain the appropriate far-field behaviour of the corresponding component of the Green's function (5.17). Since

$$\mathscr{L}_k \to \left(\frac{c_\infty}{\omega}\right)^2\left[\nabla_\perp^2 + \left(\frac{\omega}{c_\infty}\right)^2 - k^2\right] \quad \text{as } r_\perp \equiv |\boldsymbol{x}_\perp| \to \infty, \tag{6.7}$$

where

$$\nabla_\perp^2 \equiv \frac{1}{r_\perp}\frac{\partial}{\partial r_\perp}r_\perp\frac{\partial}{\partial r_\perp} + \frac{1}{r_\perp^2}\frac{\partial^2}{\partial\psi^2}, \tag{6.8}$$

ψ is the azimuthal coordinate and c_∞ is the free-stream sound speed, it follows that φ_{nl} must behave like

$$\varphi_{nl} \to \frac{1}{\sqrt{r_\perp}}\Phi_{nl}(\psi, \omega)\exp\left(-\sqrt{\kappa_n^2 - (\omega/c_\infty)^2}\,r_\perp\right) \quad \text{as } r_\perp \to \infty, \tag{6.9}$$

which means that

$$J_I \to \frac{1}{\sqrt{r_\perp}}A(X|X')\Phi(\psi)\exp\left(\mathrm{i}\left[\frac{1}{\varepsilon}\int_{X'}^{X}\kappa(X)\,\mathrm{d}X + \mathrm{i}\sqrt{\kappa^2 - \left(\frac{\omega}{c_\infty}\right)^2}\,r_\perp\right)\right] \quad \text{as } r_\perp \to \infty, \tag{6.10}$$

where we have, for simplicity, dropped the subscripts n and l.

Since φ_{nl} arises from the continuous deformation and uniform extension of the original Green's function formula (5.9), the branch cuts for the square root in (6.10) must be consistent with that result (see equation (7.2) below), which means that $\sqrt{k^2 - (\omega/c_\infty)^2}$ must be positive when $k^2 > (\omega/c_\infty)^2$ and negative imaginary when $k^2 < (\omega/c_\infty)^2$. This only occurs when the portion of the branch cut emanating from $k = \omega/c_\infty$ extends to infinity in the first quadrant and the portion emanating from $k = -\omega/c_\infty$ extends to infinity in the third quadrant. Their detailed shapes are arbitrary at this stage of the analysis.

The result may not remain bounded as $r_\perp \to \infty$ when Im $\kappa\ (X) > 0$ (i.e. when the instability wave is damped, see Tam & Burton 1984) but, as shown in § 7, it still produces an outgoing wave in the far field with this choice of branch. The only requirements are that the inner and outer solutions match and that the boundary condition at ∞ be satisfied. The outer solution eventually converts the unbounded inner solution into a propagating or damped disturbance.

The outer solution, say J_o, that is valid in the region

$$X^2 + R_\perp^2 = O(1), \tag{6.11}$$

where

$$R_\perp \equiv \varepsilon r_\perp, \tag{6.12}$$

and matches on to this result when $R_\perp \to 0$ with $X > 0$ must satisfy the reduced wave equation

$$\varepsilon^2\left(\nabla_\parallel^2 + \frac{1}{R_\perp^2}\frac{\partial^2}{\partial\psi^2}\right)J_o + \left(\frac{\omega}{c_\infty}\right)^2 J_o = 0, \tag{6.13}$$

where

$$\nabla_{\parallel}^2 \equiv \frac{1}{R_\perp}\frac{\partial}{\partial R_\perp} R_\perp \frac{\partial}{\partial R_\perp} + \frac{\partial^2}{\partial X^2}, \tag{6.14}$$

and must be of WKBJ form

$$J_o = \frac{\sqrt{\varepsilon}}{\sqrt{R_\perp}} \exp\left(\frac{\mathrm{i}}{\varepsilon}\Theta(X, R_\perp)\right)\Phi(\psi)A_o(X, R_\perp) + \ldots. \tag{6.15}$$

Substituting this into (6.13) and equating like powers of ε shows that

$$\Theta_X^2 + \Theta_{R_\perp}^2 - (\omega/c_\infty)^2 = 0 \tag{6.16}$$

and

$$2\left(\Theta_{R_\perp}\frac{\partial}{\partial R_\perp} + \Theta_X \frac{\partial}{\partial X}\right)\frac{A_o}{\sqrt{R_\perp}} + \frac{A_o}{\sqrt{R_\perp}}\nabla_{\parallel}^2\Theta = 0, \tag{6.17}$$

where the subscripts denote partial derivatives with respect to the indicated variables.

The solution to the Eikenal equation (6.16) that matches with (6.10) is

$$\Theta = \int_{X'}^{X_o} \kappa(Z)\,\mathrm{d}Z + \frac{(\omega/c_\infty)^2 R_\perp}{\mathrm{i}\sqrt{\bar{\kappa}^2 - (\omega/c_\infty)^2}}, \tag{6.18}$$

where

$$\bar{\kappa}(X, R_\perp) \equiv \kappa(X_o), \tag{6.19}$$

$$X_o \equiv X - \bar{\alpha} R_\perp \tag{6.20}$$

and

$$\bar{\alpha} \equiv \alpha(X_o) \equiv \frac{\bar{\kappa}}{\mathrm{i}\sqrt{\bar{\kappa}^2 - (\omega/c_\infty)^2}}, \tag{6.21}$$

which can be verified by differentiating (6.18) to (6.21) to obtain

$$\Theta_X = \bar{\kappa} \tag{6.22}$$

and

$$\Theta_{R_\perp} = \mathrm{i}\sqrt{\bar{\kappa}^2 - (\omega/c_\infty)^2}. \tag{6.23}$$

Expanding (6.18) in a Taylor series shows that

$$\Theta = \int_{X'}^{X} \kappa(X)\,\mathrm{d}X + \mathrm{i}\sqrt{\bar{\kappa}^2(X) - (\omega/c_\infty)^2}\,R_\perp + 0(R_\perp^2) \quad \text{as } R_\perp \to 0, \tag{6.24}$$

which, in turn, shows that (6.18) matches with the phase factor in (6.10) as $R_\perp \to 0$.

It is worth noting that $\bar{\alpha}$ satisfies the (in general complex) inviscid Burgers' equation (Burgers 1948; Pierce 1981, pp. 588–591)

$$\frac{\partial \bar{\alpha}}{\partial R_\perp} + \bar{\alpha}\frac{\partial \bar{\alpha}}{\partial X} = 0, \tag{6.25}$$

subject to the (initial) boundary condition

$$\bar{\alpha}(X, 0) = \alpha(X) \quad \text{for } X > 0. \tag{6.26}$$

The branch of the square root in (6.18) must agree with the choice of branch in (6.9) and (6.10) and must otherwise represent a continuous function of X and $R_\perp$ to the maximum possible extent. The Burgers' equation solution, which always develops a singularity when its dependent variable is real (Pierce 1981, pp. 588–591), may also

develop a singularity for complex $\bar{\alpha}$ when the mean flow Mach number is sufficiently large – corresponding to the sonic point singularity, $\bar{\kappa} = \omega/c_\infty$, in (6.19). The resulting solution would then be discontinuous across a line connecting this point to infinity, which can be made to coincide with the branch cut for the square root in (6.21) and thereby minimize the discontinuities in $\bar{\alpha}$. These discontinuities correspond to the caustics that arise in the geometric (i.e. high-frequency) acoustics (Avila & Kelle, 1963; Pierce 1981, pp. 381–384) and signify a local breakdown in the WKBJ solution (6.15), which can be eliminated by constructing a local inner solution to the reduced wave equation (6.13), but we do not pursue this issue further.

The amplitude equation (6.17) can be written more simply as

$$\frac{\partial}{\partial R_\perp} A_o^2 \frac{\partial \Theta}{\partial R_\perp} + \frac{\partial}{\partial X} A_o^2 \frac{\partial \Theta}{\partial X} = 0. \tag{6.27}$$

Inserting (6.22) and (6.23) and using (6.21) to rearrange the result shows that

$$\frac{\partial}{\partial X} \bar{\alpha}\, A_o^2 + \frac{\partial}{\partial R_\perp} A_o^2 = 0. \tag{6.28}$$

But differentiating (6.21) with respect to X shows that

$$\frac{\partial \bar{\alpha}}{\partial X} = \frac{\alpha'(X_o)}{1 + \alpha'(X_o) R_\perp}, \tag{6.29}$$

where the prime denotes differentiation with respect to the entire argument X_o. It is now easy to verify that the solution to (6.28) (and therefore (6.27)) that matches with the amplitude of (6.10) as $R_\perp \to 0$ is

$$A_o^2(X, R_\perp) = \frac{A^2(X_o|X')}{[1 + \alpha'(X_o) R_\perp]}. \tag{6.30}$$

A uniformly valid composite expansion, say $J_{I,o}$, for J that reduces to (6.6) in the inner region and (6.15) in the outer region (6.11) is (Van Dyke 1975)

$$J_{I,o} = \frac{A_{nl}(X_o|X')}{\sqrt{1 + \alpha_n'(X_o) R_\perp}} \exp\left(\frac{i}{\varepsilon} \bar{\Theta}_n(X, R_\perp)\right) \varphi_{nl}(\boldsymbol{x}_\perp) \tag{6.31}$$

where

$$\bar{\Theta}_n \equiv \Theta_n - \mathrm{i}\sqrt{\bar{\kappa}^2(X) - (\omega/c_\infty)^2}\, R_\perp. \tag{6.32}$$

Substituting this into (6.1), and using the result to replace the second term in (5.17), yields the following expression for the Green's function:

$$g_{4\sigma}^{(0)} = \int_{-\infty}^{\infty} \mathrm{e}^{-\mathrm{i}\omega(t-t')} G_{4\sigma}^{(0)}(\boldsymbol{x}|\boldsymbol{x}';\omega)\, \mathrm{d}\omega \tag{6.33}$$

where

$$G_{4\sigma}^{(0)}(\boldsymbol{x}_\perp|\boldsymbol{x}'_\perp;\omega,k,X,X') = -\int_{-\infty}^{\infty} \frac{\widetilde{c_o^2}(\boldsymbol{x}'_\perp)}{[kU(\boldsymbol{x}'_\perp) - \omega]^2} \mathrm{D}'_\sigma \mathrm{e}^{\mathrm{i}k(x_1 - x_1')} \bar{G}_o(\boldsymbol{x}_\perp|\boldsymbol{x}'_\perp)\, \mathrm{d}k$$

$$- 2\pi\mathrm{i} \sum_n \frac{\widetilde{c_o^2}(\boldsymbol{x}'_\perp) A_{nl}(X_o|X') a_{lj} \varphi_{nl}(\boldsymbol{x}_\perp)}{[\kappa_n U(\boldsymbol{x}'_\perp) - \omega]^2 \Delta_n' \sqrt{1 + \alpha_n'(X_o) R_\perp}} \mathrm{D}'_\sigma \mathrm{e}^{\mathrm{i}\bar{\Theta}_n(X, R_\perp)/\varepsilon} \varphi_{nj}(\boldsymbol{x}'_\perp), \tag{6.34}$$

the sum is over the finite number (which may be zero) of unstable eigenvalues at X' and frequency ω. $\bar{G}_o$, Δ_n', and a_{lj} are determined by solving (5.10), φ_{nl} and κ_n are obtained by solving the eigenvalue problem for the Rayleigh operator (5.11) and $\bar{\Theta}_n$, X_o, and α are given by (6.18) to (6.21), and (6.32).

7. Far-field Green's function

The primary interest is in calculating the jet noise at large distances from the flow where

$$\varepsilon r \equiv R \to \infty, \tag{7.1}$$

and the uniformly valid reduced Green's function (6.34) takes on a much simpler form. The appropriate result is derived in this section. To this end, we note that, since $\bar{G}_o$ behaves like

$$\bar{G}_o \to \frac{\exp(-\sqrt{k^2-(\omega/c_\infty)^2}\,r_\perp)}{\sqrt{r_\perp}}\mathscr{G}_o(\psi, k, \omega|\boldsymbol{x}'_\perp) \quad \text{as } r_\perp \to \infty, \tag{7.2}$$

where the choice of branch has already been discussed in conjunction with (6.9) and (6.10), the integral in the first term of (6.3) can be readily evaluated by the method of stationary phase (Carrier, Crook & Pearson 1966, p. 274) with the stationary phase point occurring at

$$\cos\theta - k[\sin\theta/\mathrm{i}\sqrt{k^2-(\omega/c_\infty)^2}] = 0 \tag{7.3}$$

or

$$k = \frac{\omega}{c_\infty}\cos\theta, \tag{7.4}$$

where θ is the polar angle

$$\tan\theta = \frac{r_\perp}{x_1} = \frac{R_\perp}{X} \tag{7.5}$$

measured relative to the downstream jet axis, and

$$R^2 \equiv X^2 + R_\perp^2 \tag{7.6}$$

is the radial coordinate.

The far-field expansion of the second term of (6.34) is evaluated in Appendix D. The results, along with (6.9) and those of this section can now be inserted into (6.34) to show that

$$G_{4\sigma}^{(0)} \to -\frac{\mathrm{e}^{\mathrm{i}\omega r/c_\infty}}{r}\sqrt{\frac{\omega}{c_\infty}\sin\theta}\left[G_{B\sigma}(\hat{\boldsymbol{x}}|\boldsymbol{x}') + \sum_n G_{I\sigma}^{(n)}(\hat{\boldsymbol{x}}|\boldsymbol{x}')\right], \tag{7.7}$$

where

$$G_{B\sigma} \equiv \frac{\sqrt{2\pi}\mathrm{i}\left[\widetilde{c_o^2}(\boldsymbol{x}'_\perp)/\omega^2\right]}{[M(\boldsymbol{x}'_\perp)\cos\theta - 1]^2}\mathrm{D}'_\sigma \exp(-\mathrm{i}\omega x'_1\cos\theta/c_\infty)\mathscr{G}_o\left(\psi, \frac{\omega}{c_\infty}\cos\theta, \omega \,|\, \boldsymbol{x}'_\perp\right), \tag{7.8}$$

$$G_{I\sigma}^{(n)} \equiv \frac{2\pi\mathrm{i}}{\sqrt{\varepsilon}}\frac{\widetilde{c_o^2}(\boldsymbol{x}'_\perp)A_{nl}(\bar{\alpha}_{o,n}|X')a_{lj}\Phi_{nl}(\psi)}{[\kappa_n U(\boldsymbol{x}'_\perp) - \omega]^2\Delta'_n\sqrt{\kappa'_n(\bar{\alpha}_{on})}}\mathrm{D}'_\sigma \exp(\mathrm{i}\Theta_n^\infty(\theta, X')/\varepsilon)\varphi_{nj}(\boldsymbol{x}'_\perp), \tag{7.9}$$

$\hat{\boldsymbol{x}} = \hat{\boldsymbol{x}}(\theta, \psi)$ denotes the unit vector in the $\boldsymbol{x}$-direction,

$$\Theta_n^\infty(\theta, X') \equiv \int_{X'}^{\bar{\alpha}_{on}} \kappa_n(Z)\,\mathrm{d}Z - \frac{\omega}{c_\infty}\bar{\alpha}_{on}\cos\theta; \tag{7.10}$$

$\bar{\alpha}_{on}$ is determined implicitly by (D 2), (D 3), and (D 7) once the local growth rate $\kappa_n(X, \omega)$ is determined from the eigenvalue problem (C 8), and

$$M(\boldsymbol{x}'_\perp) \equiv U(\boldsymbol{x}'_\perp)/c_\infty \tag{7.11}$$

is the acoustic Mach number. Appendix D also shows that (6.15) exhibits the desired outgoing wave behaviour at infinity.

8. The acoustic spectra

Jet noise theory is primarily concerned with predicting the acoustic spectrum, which corresponds to the Fourier transform of mean-square pressure correlation

$$\overline{p^2} \equiv \frac{1}{2T}\int_{-T}^{T} p_o'(\boldsymbol{x},t)p_o'(\boldsymbol{x},t+t_o)\,\mathrm{d}t \tag{8.1}$$

in the far field where $r\to\infty$ and p_o', which is defined by (2.11), reduces to the pressure fluctuation. Here, T denotes a large time interval. A relatively simple formula for this entity is obtained in this section.

Inserting (4.6) into (8.1) and changing the integration variables to $t_1 \equiv t - t''$ and $\tau \equiv t'' - t'$, yields

$$\begin{aligned}\overline{p^2} &= \frac{1}{2T}\int_{-T}^{T}\iint_{-\infty}^{\infty}\iint_{V}\gamma_{i\sigma}(\boldsymbol{x}|\boldsymbol{x}',t+t_o-t')\gamma_{j\mu}(\boldsymbol{x}|\boldsymbol{x}'',t-t'')\\ &\quad\times\tau_{\sigma i}(\boldsymbol{x}',t')\tau_{\mu j}(\boldsymbol{x}'',t'')\,\mathrm{d}\boldsymbol{x}'\,\mathrm{d}\boldsymbol{x}''\,\mathrm{d}t'\,\mathrm{d}t''\,\mathrm{d}t\\ &= \iint_{-\infty}^{\infty}\iint_{V}\gamma_{i\sigma}(\boldsymbol{x}|\boldsymbol{x}',t_1+t_o+\tau)\gamma_{j\mu}(\boldsymbol{x}|\boldsymbol{x}'',t_1)\bar{\tau}_{\sigma i\mu j}(\boldsymbol{x}',\boldsymbol{x}''-\boldsymbol{x}',\tau)\,\mathrm{d}\boldsymbol{x}'\,\mathrm{d}\boldsymbol{x}''\,\mathrm{d}t_1\,d\tau,\end{aligned} \tag{8.2}$$

where

$$\bar{\tau}_{\sigma i\mu j}(\boldsymbol{x}';\boldsymbol{x}''-\boldsymbol{x}',\tau) \equiv \frac{1}{2T}\int_{-T}^{T}\tau_{\sigma i}(\boldsymbol{x}',t')\tau_{\mu j}(\boldsymbol{x}'',t'+\tau)\,\mathrm{d}t' \tag{8.3}$$

is the density-weighted fourth-order two-point time-delayed turbulent velocity/total enthalpy correlation. Inserting (4.8), with $\sigma_{\mu j}' = 0$, into this result shows that

$$\bar{\tau}_{\sigma i\mu j} = \overline{\tau_{\sigma i\mu j}'}(\boldsymbol{x}';\boldsymbol{x}''-\boldsymbol{x}',\tau) - \overline{\tau_{\sigma i}'}(\boldsymbol{x}';\boldsymbol{0},0)\overline{\tau_{\mu j}'}(\boldsymbol{x}'';\boldsymbol{0},0), \tag{8.4}$$

where

$$\begin{aligned}\overline{\tau_{\sigma i\mu j}'}(\boldsymbol{x}';\boldsymbol{x}''-\boldsymbol{x}',\tau) \equiv \frac{1}{2T}\int_{-T}^{T}&\rho(\boldsymbol{x}',t')\,\rho(\boldsymbol{x}'',t'+\tau)\\ &\times v_\sigma'(\boldsymbol{x}',t')v_i'(\boldsymbol{x}',t')v_\mu'(\boldsymbol{x}'',t'+\tau)v_j'(\boldsymbol{x}'',t'+\tau)\,\mathrm{d}t'\end{aligned} \tag{8.5}$$

and

$$\overline{\tau_{\sigma i}'}(\boldsymbol{x}';\boldsymbol{x}''-\boldsymbol{x}',\tau) \equiv \frac{1}{2T}\int_{-T}^{T}\rho(\boldsymbol{x}',t')v_\sigma'(\boldsymbol{x}',t')v_i'(\boldsymbol{x}'',t'+\tau)\,\mathrm{d}t' \tag{8.6}$$

are the fourth- and second-order correlations of the fluctuating (i.e. turbulence) velocities or total enthalpy. Notice that

$$\tilde{T}_{\sigma j}(\boldsymbol{x}') = -\overline{\tau_{\sigma j}'(\boldsymbol{x}',\boldsymbol{0},0)}. \tag{8.7}$$

Equation (8.2) can be written more compactly as

$$\overline{p^2}(\boldsymbol{x},t_o) = \int_{-\infty}^{\infty}\iint_{V}\bar{\gamma}_{j\sigma l\mu}(\boldsymbol{x}|\boldsymbol{x}',\boldsymbol{\eta},t_o+\tau)\bar{\tau}_{\sigma j\mu l}(\boldsymbol{x}';\boldsymbol{\eta},\tau)\,\mathrm{d}\boldsymbol{x}'\,\mathrm{d}\boldsymbol{\eta}\,\mathrm{d}\tau, \tag{8.8}$$

where

$$\bar{\gamma}_{j\sigma l\mu} \equiv \int_{-\infty}^{\infty}\gamma_{j\sigma}(\boldsymbol{x}|\boldsymbol{x}',t_1+t_o+\tau)\gamma_{l\mu}(\boldsymbol{x}|\boldsymbol{x}'+\boldsymbol{\eta},t_1)\,\mathrm{d}t_1, \tag{8.9}$$

which can be expressed in terms of the Green's function, accounts for the acoustic propagation and mean flow interaction effects. These results provide a direct linear relation between the mean-square acoustic pressure and the fourth-order correlation of the turbulent fluctuations in the jet. Unfortunately, determining this latter quantity,

either experimentally or numerically, is a very difficult task and it is, therefore, highly desirable to make the acoustic predictions as insensitive to its details as possible. In fact, this is one of the main reasons for using the moving-media acoustic analogies rather than the simpler Lighthill formulation. This desensitization would certainly be enhanced if the variation of $\bar{\tau}_{\sigma j\mu l}$ with $\boldsymbol{\eta}$ was much more rapid than that of the propagation factor $\bar{\gamma}_{j\sigma l\mu}$, because the latter could then be treated as a constant relative to the $\boldsymbol{\eta}$-integration and the result would then depend only on the integral of $\bar{\tau}_{\sigma j\mu l}$ over the separation variable $\boldsymbol{\eta}$, which, in turn, depends only on the decay time τ at any given source point $\boldsymbol{x}'$. This may be the case at lower Mach numbers, but the η_1-decay rate is expected to be much slower at the higher Mach numbers of technological interest. However, Lighthill (1952, 1954) pointed out that the streamwise decay rate should be much more rapid in a reference frame moving with the convection velocity, U_c, of the turbulence and Ffowcs Williams (1963) showed that this idea can best be implemented by introducing a moving frame correlation, say

$$\tau^{M}_{\sigma j\mu l}(\boldsymbol{x}', \boldsymbol{\xi}, \tau) \equiv \bar{\tau}_{\sigma j\mu l}(\boldsymbol{x}', \boldsymbol{\eta}, \tau) \tag{8.10}$$

where

$$\boldsymbol{\xi} \equiv \boldsymbol{\eta} - \hat{\boldsymbol{i}}\, U_c\, \tau, \tag{8.11}$$

before integrating the turbulence correlation over the separation vector. Introducing this into (8.8) and changing the integration variable to $\boldsymbol{\xi}$ (not to be confused with the ξ introduced in Appendix D) yields

$$\overline{p^2}(\boldsymbol{x}, t_o) = \int_{-\infty}^{\infty} \iint_{V} \bar{\gamma}_{j\sigma l\mu}(\boldsymbol{x}|\boldsymbol{x}', \boldsymbol{\xi} + \hat{\boldsymbol{i}}\, U_c\tau,\ t_o + \tau)\tau^{M}_{\sigma j\mu l}(\boldsymbol{x}'; \boldsymbol{\xi}, \tau)\, \mathrm{d}\boldsymbol{x}'\, \mathrm{d}\boldsymbol{\xi}\, \mathrm{d}\tau. \tag{8.12}$$

This is a generalization of the result obtained by Ffowcs Williams (1963) in the Lighthill context. It turns out to be much simpler in frequency space when the observation point $\boldsymbol{r}$ is in the far field.

To obtain the appropriate result, we introduce the far-field acoustic spectrum

$$I_\omega(\boldsymbol{x}) \equiv \frac{1}{2\pi} \int_{-\infty}^{\infty} \mathrm{e}^{\mathrm{i}\omega t_o}\, \overline{p^2}(\boldsymbol{x}, t_o)\, \mathrm{d}t_o, \tag{8.13}$$

note that the Fourier transform of a correlation, say $\int_{-\infty}^{\infty} f(t+\tau)g(\tau)\, \mathrm{d}\tau$, is just $2\pi F(\omega)G^*(\omega)$ (where capital letters denote Fourier transforms of the corresponding lower-case letters, and the asterisk denotes complex conjugates), and take the Fourier transform to (8.12) to obtain

$$I_\omega(\boldsymbol{x}|\boldsymbol{x}') = 2\pi \int_{-\infty}^{\infty} \int_{V} \Gamma_{j\sigma}(\boldsymbol{x}|\boldsymbol{x}'; \omega)\Gamma^*_{l\mu}(\boldsymbol{x}|\boldsymbol{x}' + \boldsymbol{\xi} + \hat{\boldsymbol{i}}\, U_c\tau; \omega)\, \mathrm{e}^{-\mathrm{i}\omega\tau}\, \tau^{M}_{\sigma j\mu l}(\boldsymbol{x}', \boldsymbol{\xi}, \tau)\, \mathrm{d}\boldsymbol{\xi}\, \mathrm{d}\tau, \tag{8.14}$$

where the left-hand side is defined by

$$I_\omega(\boldsymbol{x}) = \int_{V} I_\omega(\boldsymbol{x}|\boldsymbol{x}')\, \mathrm{d}\boldsymbol{x}' \tag{8.15}$$

and therefore denotes the acoustic spectrum at $\boldsymbol{x}$ due to a unit volume of turbulence at $\boldsymbol{x}'$.

Now it is clear from (4.7), (6.33), and (7.7) to (7.9) that

$$\Gamma_{j\sigma} = -\frac{\mathrm{e}^{\mathrm{i}\omega r/c_\infty}}{r} \sqrt{\frac{\omega}{c_\infty} \sin\theta} \left[\Gamma_{Bj\sigma}(\hat{\boldsymbol{x}}|\boldsymbol{x}') + \sum_{n} \Gamma^{(n)}_{Ij\sigma}(\hat{\boldsymbol{x}}|\boldsymbol{x}') \right], \tag{8.16}$$

where

$$\Gamma_{Bj\sigma} = \tilde{\Gamma}_{Bj\sigma}(\hat{\boldsymbol{x}}|\boldsymbol{x}'_\perp)\exp\left(-\frac{\omega}{c_\infty}x'_1\cos\theta\right) = \tilde{\mathrm{D}}_{j\sigma\mu}G_{B\mu}(\hat{\boldsymbol{x}}|\boldsymbol{x}'), \tag{8.17}$$

$$\Gamma^{(n)}_{Ij\sigma} = \tilde{\Gamma}^{(n)}_{Ij\sigma}(\hat{\boldsymbol{x}}|\boldsymbol{x}'_\perp)\exp\left(\frac{\mathrm{i}}{\varepsilon}\Theta^\infty_n(\theta, x')\right) = \tilde{\mathrm{D}}_{j\sigma\mu}G^{(n)}_{I\mu}(\hat{\boldsymbol{x}}|\boldsymbol{x}') \tag{8.18}$$

and (for the small spread rate being considered here)

$$\tilde{\mathrm{D}}_{j\sigma\mu} \equiv -\delta_{\sigma\mu}\frac{\partial}{\partial x'_j} + \frac{(\gamma-1)}{2}\left(2\frac{\partial U}{\partial x'_j}\delta_{\sigma 1}\,\delta_{\mu 4} + \delta_{j\sigma}\frac{\partial}{\partial x'_\mu}\right). \tag{8.19}$$

provided θ and M are sufficiently large.

Since Θ^∞ varies on the slow streamwise length scale X', which is much larger than the correlation length of the turbulence, we can account for its variation over the range of integration in (8.14) by expanding it in a Taylor series and using (6.22) to show that

$$\Theta^\infty(\theta, X' + \varepsilon(\xi_1 + U_c\tau)) = \Theta^\infty(\theta, X') - \varepsilon\kappa(X')(\xi_1 + U_c\tau) + \ldots \tag{8.20}$$

with more than enough accuracy to evaluate (8.14). It therefore follows from (8.17) and (8.18) that

$$\Gamma_{Bj\sigma}(\hat{\boldsymbol{x}}|\boldsymbol{x}' + \boldsymbol{\xi} + \hat{\boldsymbol{i}}\,U_c\tau) = \Gamma_{Bj\sigma}(\hat{\boldsymbol{x}}|\boldsymbol{x}' + \boldsymbol{\xi})\,\mathrm{e}^{-\mathrm{i}\omega M_c\cos\theta\tau}, \tag{8.21}$$

$$\Gamma^{(n)}_{Ij\sigma}(\hat{\boldsymbol{x}}|\boldsymbol{x}' + \boldsymbol{\xi} + \hat{\boldsymbol{i}}\,U_c\tau) = \Gamma^{(n)}_{Ij\sigma}(\hat{\boldsymbol{x}}|\boldsymbol{x}' + \boldsymbol{\xi})\,\mathrm{e}^{-\mathrm{i}\kappa_n(X')U_c\tau}, \tag{8.22}$$

where $M_c = U_c/c_\infty$ denotes the convective Mach number.

For simplicity, we only consider the case where a single mode is excited at $\boldsymbol{x}'$ and ω. Other modes will, of course, be excited at lower frequencies and will have to be accounted for in order to predict the true acoustic spectrum. Then inserting these into (8.14) via (8.16) shows that

$$\begin{aligned} I_\omega(\boldsymbol{x}|\boldsymbol{x}') = \left(\frac{2\pi}{r}\right)^2\frac{\omega}{c_\infty}\sin\theta\int_V &[\Gamma_{Bj\sigma}(\hat{\boldsymbol{x}}|\boldsymbol{x}') + \Gamma_{Ij\sigma}(\hat{\boldsymbol{x}}|\boldsymbol{x}')] \\ &\times [\Gamma^*_{Bl\mu}(\hat{\boldsymbol{x}}|\boldsymbol{x}' + \boldsymbol{\xi})H^*_{\sigma j\mu l}(\boldsymbol{x}'; \boldsymbol{\xi}, \omega(1 - M_c\cos\theta)) \\ &+ \Gamma^*_{Il\mu}(\hat{\boldsymbol{x}}|\boldsymbol{x}' + \boldsymbol{\xi})H^*_{\sigma j\mu l}(\boldsymbol{x}'; \boldsymbol{\xi}, \omega - U_c\kappa^*(X', \omega))]\,\mathrm{d}\boldsymbol{\xi} \quad \text{for } r \gg 1, \end{aligned} \tag{8.23}$$

where

$$H_{\sigma j\mu l}(\boldsymbol{x}'; \boldsymbol{\xi}, \omega) \equiv \frac{1}{2\pi}\int_{-\infty}^{\infty}\mathrm{e}^{\mathrm{i}\omega\tau}\tau^M_{\sigma j\mu l}(\boldsymbol{x}'; \boldsymbol{\xi}, \tau)\,\mathrm{d}\tau \tag{8.24}$$

denotes the two-point fourth-order turbulence spectrum relative to the moving frame.

This result is, aside from the easily relaxed constraint of single mode excitation, nearly exact. The only significant approximation is that the mean flow spread, ε, is small. But $H_{\sigma j\mu l}$ is expected to vary much more rapidly with $\boldsymbol{\xi}$ than $\Gamma_{l\mu}$ and (8.23) can therefore be approximated by

$$\begin{aligned} I_\omega(\boldsymbol{x}|\boldsymbol{x}') = \left(\frac{2\pi}{r}\right)^2\frac{\omega}{c_\infty}\sin\theta\,&[\Gamma_{Bj\sigma}(\hat{\boldsymbol{x}}|\boldsymbol{x}') + \Gamma_{Ij\sigma}(\hat{\boldsymbol{x}}|\boldsymbol{x}')] \\ \times [\Gamma^*_{Bl\mu}(\hat{\boldsymbol{x}}|\boldsymbol{x}')\Psi^*_{\sigma j\mu l}(\boldsymbol{x}'; \omega(1 - M_c\cos\theta)) &+ \Gamma^*_{Il\mu}(\hat{\boldsymbol{x}}|\boldsymbol{x}')\Psi^*_{\sigma j\mu l}(\boldsymbol{x}'; \omega - U_c\kappa^*(X', \omega))] \end{aligned} \tag{8.25}$$

where

$$\Psi_{\sigma j\mu l}(\boldsymbol{x}';\omega) \equiv \int_V H_{\sigma j\mu l}(\boldsymbol{x}';\boldsymbol{\xi},\omega)\,\mathrm{d}\boldsymbol{\xi} \tag{8.26}$$

is the single-point fourth-order turbulence spectrum at $\boldsymbol{x}'$.

This approximation is also invalid when $M_c\cos\theta = 1$ because the first spectral function in (8.25) does not go to zero as $\omega \to \infty$ in this case, which causes the integral of (8.25) with respect to ω and therefore the mean-square pressure to become infinite. Ffowcs Williams (1963) showed that this difficulty could be overcome within the Lighthill (1952) context by replacing the Doppler factor $(1 - M_c\cos\theta)$ by $\sqrt{(1 - M_c\cos\theta)^2 + (a\,M_c)^2}$ where a is a relatively small constant. This result does not remain valid in the present more general context, but our interest here is in the case where $M_c < 1$.

9. A specific example

To make these results more concrete, we consider the case of an axisymmetric mean flow, i.e. a round jet, where

$$U = U(r_\perp, X), \quad \widetilde{c_o^2} = \widetilde{c_o^2}(r_\perp, X) \tag{9.1}$$

and $\boldsymbol{V}$ is purely radial with magnitude $V(r_\perp, X)$. Then the mean flow equations (A 7), (A 8), and (A 10) decouple from (A 9), i.e. they reduce to the usual boundary-layer equations, but with D_o now given by

$$\mathrm{D}_o = \frac{\partial}{\partial X}U + \frac{1}{r_\perp}\frac{\partial}{\partial r_\perp}r_\perp V \tag{9.2}$$

in place of (A 11) and S given by

$$S = \frac{\partial}{\partial X}\left(T_{11}^{(0)} - P\right) + \frac{1}{r}\frac{\partial}{\partial r}rT_{1r}^{(1)} \tag{9.3}$$

in place of (A 12). The radial pressure equation (A 6) reduces to

$$\frac{\partial\left(P - T_{rr}^{(0)}\right)}{\partial r_\perp} = \frac{T_{rr}^{(0)} - T_{\theta\theta}^{(0)}}{r_\perp}, \tag{9.4}$$

which can be used to eliminate P in (9.3), and the Reynolds stress components are defined in the obvious way. However, the $\partial/\partial X(T_{11}^{(0)} - P)$ term is fairly small and is usually considered to be negligible (Pope 2000, p. 114). This does not cause any inconsistency in the asymptotic results and we shall suppose this approximation to be valid.

The Rayleigh operator (5.11) now becomes

$$\mathscr{L}_k = \frac{1}{r_\perp}\frac{\partial}{\partial r_\perp}\frac{r_\perp\widetilde{c_o^2}}{(kU-\omega)^2}\frac{\partial}{\partial r_\perp} - \frac{\widetilde{c_o^2}}{(kU-\omega)^2}\left(k^2 - \frac{1}{r_\perp^2}\frac{\partial^2}{\partial\psi^2}\right) + 1 \tag{9.5}$$

and $\bar{G}_o$ must therefore be of the form

$$\bar{G}_o = \sum_{n=-\infty}^{\infty} \mathrm{e}^{\mathrm{i}n(\psi-\psi')}G^{(n)}(r_\perp|r'_\perp), \tag{9.6}$$

where

$$\mathscr{L}_{nk}G^{(n)} = \frac{\delta(r_\perp - r'_\perp)}{(2\pi)^2 r_\perp} \tag{9.7}$$

and

$$\mathscr{L}_{nk} \equiv \frac{1}{r_\perp}\frac{\mathrm{d}}{\mathrm{d}r_\perp}\frac{r_\perp \tilde{c}_o^2}{(kU-\omega)^2}\frac{\mathrm{d}}{\mathrm{d}r_\perp} + \left[1 - \frac{\tilde{c}_o^2}{(kU-\omega)^2}\left(k^2 + \frac{n^2}{r_\perp^2}\right)\right]. \tag{9.8}$$

It follows that

$$G^{(n)} = \frac{w_n^{(1)}(r_\perp, k)w_n^{(2)}(r'_\perp, k)}{\Delta_n(k)} \quad \text{(no sum on } n\text{)} \tag{9.9}$$

for $r_\perp > r'_\perp$(with a similar equation holding, but with $r_\perp$and $r'_\perp$interchanged when $r_\perp < r'$), where

$$\mathscr{L}_{nk}w_n^{(l)}(r_\perp, k) = 0 \quad \text{for } l = 1, 2, \tag{9.10}$$

$$w_n^{(1)} \sim \frac{1}{\sqrt{r_\perp}}\mathrm{e}^{-\sqrt{k^2-(\omega/c_\infty)^2}\,r_\perp} \quad \text{as } r_\perp \to \infty, \tag{9.11}$$

$$w_n^{(2)} \to r_\perp^{|n|} \quad \text{as } r_\perp \to 0, \tag{9.12}$$

and

$$\Delta_n \equiv -(2\pi)^2 r_\perp \tilde{c}_o^2 W_n/(kU-\omega)^2, \tag{9.13}$$

where

$$W_n \equiv w_n^{(1)}\frac{\mathrm{d}}{\mathrm{d}r_\perp}w_n^{(2)} - w_n^{(2)}\frac{\mathrm{d}}{\mathrm{d}r_\perp}w_n^{(1)} \tag{9.14}$$

is the Wronskian of $w_n^{(1)}$ and $w_n^{(2)}$, and is independent of $r_\perp$.

Since κ_n depends on n^2, the eigenvalue problem for $\mathscr{L}_k$ is doubly degenerate for each n^2 (corresponding to $\pm n$)

$$\varphi_{nj} \to \varphi_{n\pm} \equiv w_n^{(2)}(r_\perp, \kappa_n)\mathrm{e}^{\pm \mathrm{i}n\psi}, \tag{9.15}$$

and a_{lj} is equal to 1 for $l \neq j$ and zero otherwise. The constant Δ'_n that appears in (5.17), (6.1), (6.34), and (7.9) is now the derivative of (9.13) with respect to k,

$$\Delta'_n = \lim_{k \to \kappa_n}\frac{\mathrm{d}\Delta_n(k)}{\mathrm{d}k} \tag{9.16}$$

evaluated at κ_n and it follows from (7.2), (9.6), (9.9), and (9.11) that Φ_{nl} (defined implicitly by (6.9)) and the function $\mathscr{G}_o$ in (7.2) are given by

$$\Phi_{nl} \to \Phi_{n\pm} \equiv \mathrm{e}^{\pm \mathrm{i}n\psi} \tag{9.17}$$

and

$$\mathscr{G}_o = \sum_{n=-\infty}^{\infty}\frac{\mathrm{e}^{\mathrm{i}n(\psi-\psi')}}{\Delta_n}w_n^{(2)}(r'_\perp). \tag{9.18}$$

All other quantities in (7.8) and (7.9) can be calculated from the preceding equations once the eigenvalue and boundary value problems for the operators $\mathscr{L}_{nk}$ have been solved.

10. Some approximate results

Equation (8.25) is very general and relatively exact but a great deal of modelling and/or computation is required to evaluate all of its terms. It is therefore worthwhile

to introduce some approximations that can be used to gain insight into the importance of the various physical effects described by this result, which will be done in this section.

Considerable simplification can be achieved by assuming that

$$\Psi_{\sigma j\mu l}(\omega) \simeq \delta_{\sigma j}\delta_{\mu l}\Psi_o(\omega), \tag{10.1}$$

which implies, among other things, that $h_0' \simeq 0$. It follows from (7.8), (7.9), (8.17), (8.18), and (8.19) that

$$\Gamma_{Bjj} = -\frac{5-3\gamma}{2}\sqrt{2\pi\mathrm{i}}\frac{\partial}{\partial x_j'}\frac{\widetilde{c_o^2}(x_\perp')/\omega^2}{[M(\boldsymbol{x}_\perp')\cos\theta - 1]^2}\frac{\partial}{\partial x_j'}\exp\left(-\mathrm{i}\frac{\omega}{c_\infty}x_1'\cos\theta\right)$$
$$\times \mathscr{G}_o\left(\psi, \frac{\omega}{c_\infty}\cos\theta|\boldsymbol{x}_\perp'\right) = \frac{5-3\gamma}{2}\sqrt{2\pi\mathrm{i}}\exp\left(-\mathrm{i}\frac{\omega}{c_\infty}x_1'\cos\theta\right)\mathscr{G}_o\left(\varphi, \frac{\omega}{c_\infty}\cos\theta|\boldsymbol{x}_\perp'\right) \tag{10.2}$$

and, again assuming only a single excited mode,

$$\Gamma_{Ijj} = \frac{2\pi\mathrm{i}}{\sqrt{\varepsilon}}\frac{5-3\gamma}{2}\frac{A(\bar{\alpha}_o|X')\Phi(\psi)}{\Delta'\sqrt{\kappa'(\bar{\alpha}_o)}}\mathrm{e}^{\mathrm{i}\Theta^\infty(\theta,X')/\varepsilon}\varphi(\boldsymbol{x}_\perp') \tag{10.3}$$

when ω is less than the neutral frequency at X' ($\mathrm{Im}\,\kappa(\omega, X=0)$ and equal to zero otherwise. Then, using (10.1) and neglecting the cross-coupling terms in (8.25) yields

$$I_\omega(\boldsymbol{x}|\boldsymbol{x}') \simeq \left[\frac{5-\gamma 3}{2r}\right]^2\frac{\omega}{c_\infty}\sin\theta\left[2\pi|\mathscr{G}_o|^2\Psi_o(\omega(1-M_c\cos\theta))\right.$$
$$\left.+\left|\frac{2\pi\varphi(\boldsymbol{x}_\perp')\Phi(\psi)A(\bar{\alpha}_o)}{\Delta'\sqrt{\kappa'(\bar{\alpha}_o)}}\right|^2\mathrm{e}^{\mathrm{i}(\Theta^\infty-\Theta^{\infty *})/\varepsilon}\Psi_o^*(\omega - U_c\kappa^*(X',\omega))\right]. \tag{10.4}$$

11. Some numerical results

In this section, we carry out some numerical computations based on (10.4). Low-Reynolds-number direct numerical simulations (Freund 2002) suggest that Ψ_o can be fairly well represented by a modified Gaussian distribution, say

$$\Psi_o = \frac{l_s^3 a_s}{\omega_s}\left(\frac{\rho_s u_s^2}{4\pi}\right)^2\mathrm{e}^{-(\omega/2\omega_s)^2}\left[1+b_s\left(\frac{\omega}{\omega_s}\right)^6\right]^{-1}, \tag{11.1}$$

where ρ_s is a constant representing a characteristic density, ω_s is a frequency (inverse time) scale of the turbulence, $l_s \propto X'$ is a characteristic length scale, $u_s \propto 1/X'$ is a characteristic turbulent velocity, and a_s, b_s are empirically determined scale functions.

The experiments show that the mean velocity is reasonably well represented by (Tam & Burton 1984)

$$U/U_{cl} = \bar{U}(\bar{\eta})/\hat{U}_{cl}(X'), \tag{11.2}$$

with

$$\bar{\eta} \equiv r_\perp/X' \tag{11.3}$$

over much of the jet.

Pope (2000, p. 116) shows that this type of solution is consistent with the mean flow equations (A 7) – (A 10), for the axisymmetric case being considered here. When $\hat{U}_{cl}$ = const., the Rayleigh stability equation solutions depend on the frequency and the local streamwise coordinate only as the product $\bar{\omega} \equiv \omega X'$. We expect $\hat{U}_{cl}$ to

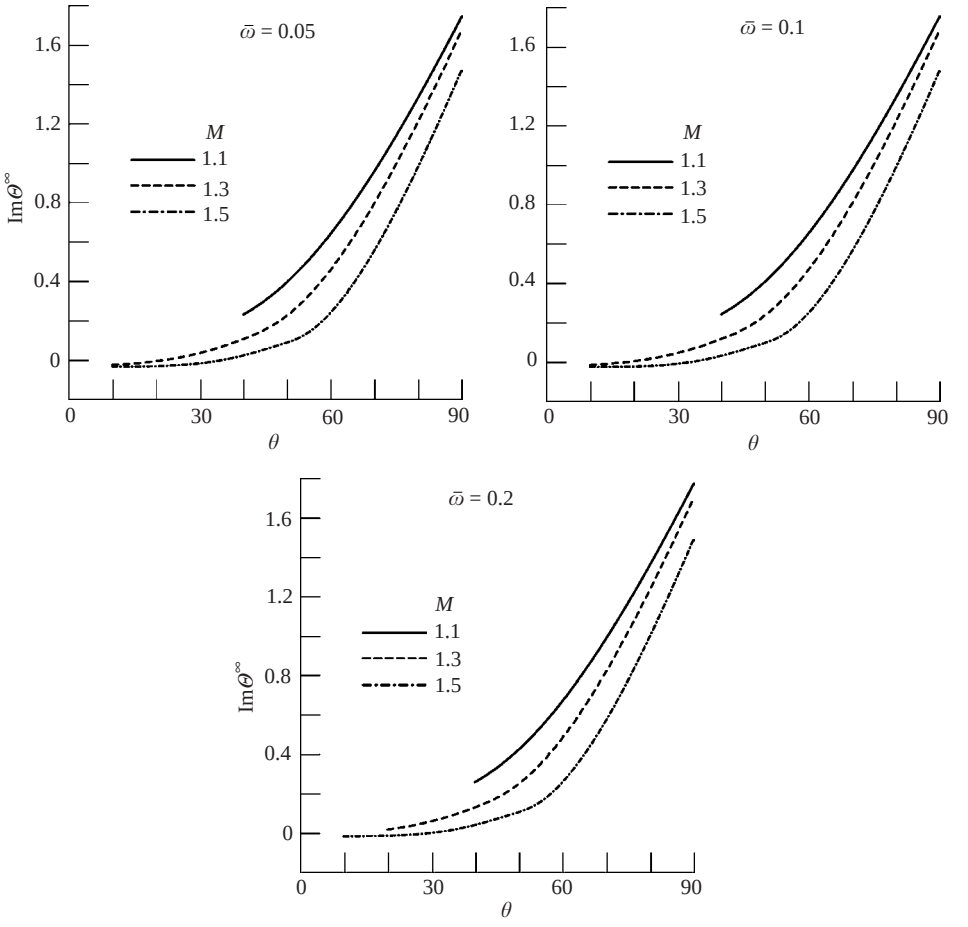

FIGURE 4. Plot of $\mathrm{Im}\Theta^{\infty}$ vs. θ for $n = 0$. $M = 1.1$ (solid), $M = 1.3$ (dashed), $M = 1.5$ (dot-dash).

be nearly constant up to the end of the potential core (see figures 5 and 6 of Tam & Burton 1984) and take $\bar{U}$ to be of the form

$$\bar{U}(\bar{\eta}) = \tfrac{1}{2}[1 - \tanh b_2(\bar{\eta} - 1)] \tag{11.4}$$

in this region. $\bar{\eta} = 1$ is the centreline of the shear layer and the hyperbolic tangent changes rapidly enough to ensure that $\bar{U}(0)$ is reasonably close to unity. The mean sound speed profile is taken to be uniform and equal to its ambient value. While the present formulation is intended to minimize the dependence of the results on the details of the turbulence, the actual sound field is expected to be strongly source dependent and the numerical computations based on this simple flow model should only provide a qualitative indication of the probable experimental results.

The imaginary part of the phase factor Θ^{∞}in the second term in (10.4) arises from the WKBJ solution and accounts for the initial transverse decay of the instability before it turns into a propagating disturbance. This term will be negligibly small (compared to the first) when Im Θ^{∞} is$O(1)$ and greater than zero, and very large (i.e. it will be dominant) when Im Θ^{∞} is$O(1)$ and less than zero, since the spread rate ε is very small (of the order of 0.1). Figures 4–6 are plots of Im Θ^{∞} as a function

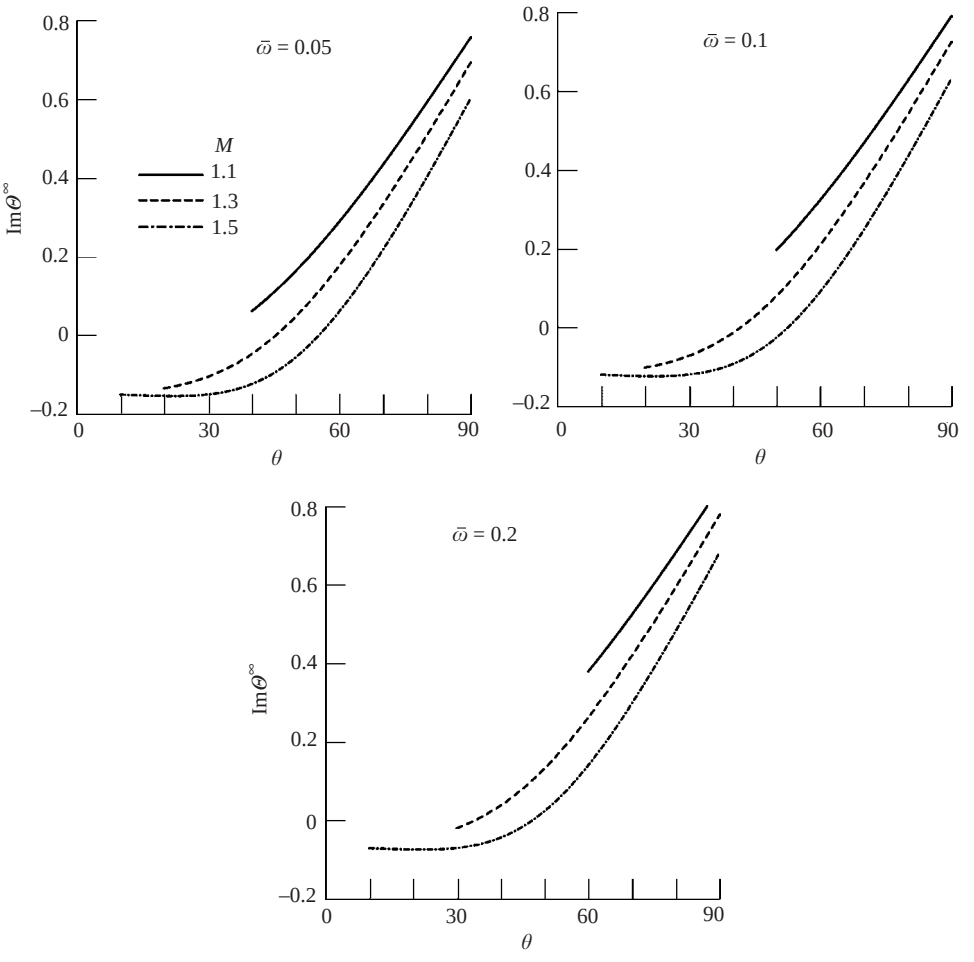

FIGURE 5. As figure 4 but for $n = 1$.

of θ for various values of the Mach number M and source frequency $\bar{\omega}$ for the first three azimuthal instability modes. It shows that Im Θ^{∞} is always positive at $\theta = 90^{\circ}$ but can cross the axis and become negative when θ is sufficiently small and M is sufficiently large. The results suggest that the $n = 1$ azimuthal mode will make the largest contribution to the instability wave component of the Green's function, and that its magnitude will be greater at lower frequencies.

The curves are truncated at certain relatively small values of θ, because $\bar{\alpha}$ does not exhibit the asymptotic behaviour (D 1) and (D 2) beyond these points and the second term becomes non-radiating (i.e. evanescent) there. The 90° spectral shape is therefore produced by the first term in (10.4), which as noted above, corresponds to the usual Lilley equation solutions that appear in the literature and is primarily determined by the factor $(\omega/c_{\infty})^4 \Psi_o(\omega(1 - M_c \cos\theta)) = (\omega/c_{\infty})^4 \Psi_o(\omega)$ at that angle. It has a similar shape at all other angles but its magnitude increases and its frequency scale is stretched when $\theta < 90^{\circ}$ – implying that the spectral peak moves to higher frequencies as $\theta \to 0$, which is not consistent with experimental observations (e.g. Tam *et al.* 1996; also see figure 7(*a*) of Freund 2002).

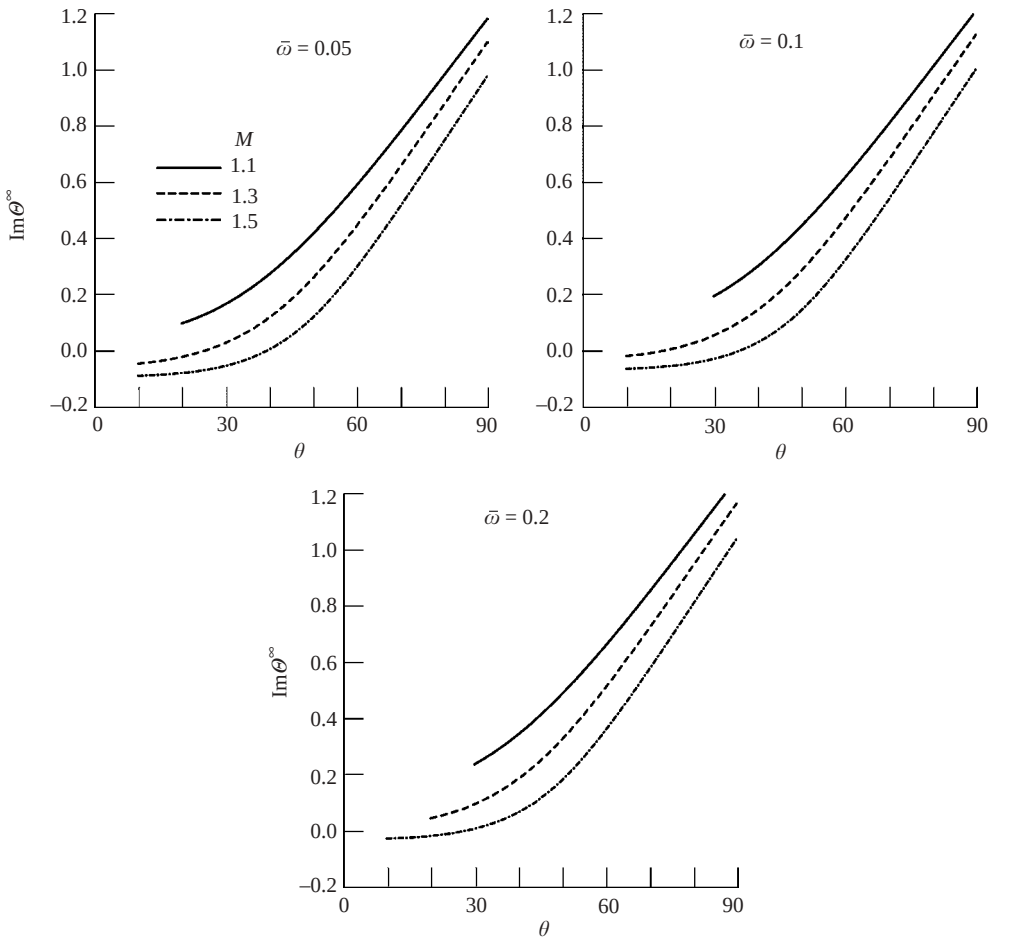

FIGURE 6. As figure 4 but for $n = 2$.

Some typical measurements taken from Norum (1994) are shown in figure 7. The jet Mach number is approximately 1.5 and the flow is fully expanded – which means that there is very little shock-associated noise in this case. Notice that the peak of the small-angle spectrum is at a much lower frequency than that at 90°. When Lilley's equation was first introduced (Lilley 1974) the expectation was that this behaviour would be produced by the refraction effects that are included in the conventional bounded solution (which corresponds to the first term in (10.4)) – the argument being that they would cut off the high-frequency part of the spectrum at small angles to the downstream axis and thereby cause an apparent shift to lower frequencies. But our numerical results (as well as those of Khavaran & Bridges 2004) show that all the relevant frequencies are equally reduced by refraction at the higher Mach numbers being considered here and the net result is an increase in the peak frequency of this spectrum – which is just the opposite of what is shown in figure 7. But figures 4 – 6 show that the second term can become dominant at these angles when M is sufficiently large. Its spectral shape is relatively independent of angle and has a much narrower width than $\Psi_o(\omega)$ due to the relatively narrow band of unstable frequencies at X'.

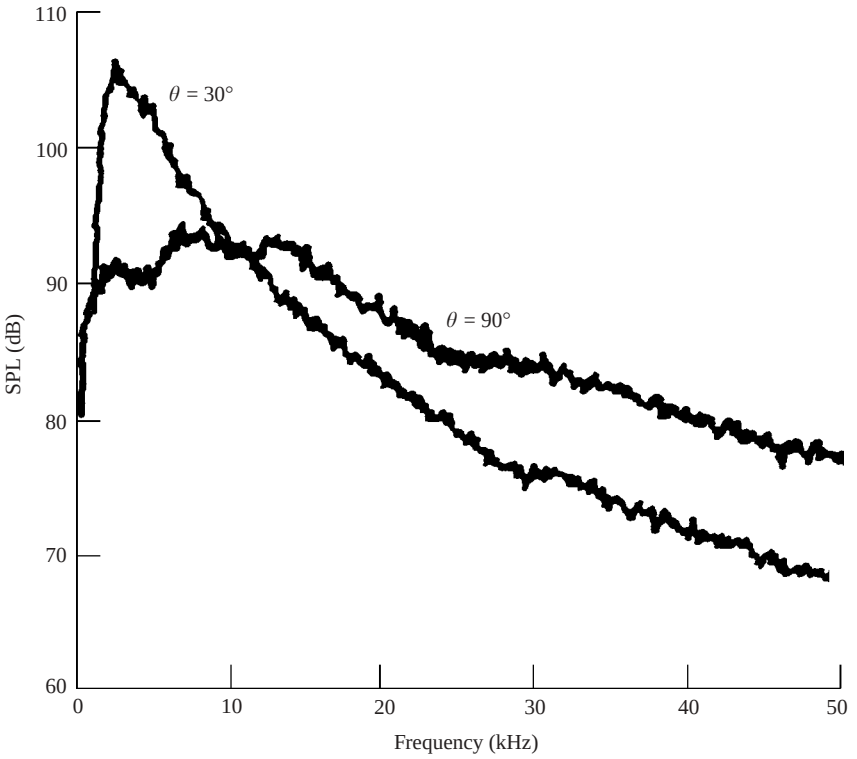

FIGURE 7. Measurements of the far-field acoustic spectra at $\theta = 90°$ and $\theta = 30°$ from Norum (1994).

The argument, $\omega - U_c\kappa(X', \omega)$, of Ψ_o tends to be close to zero over most of this range (where the second term is dominant), which means that the resulting acoustic spectrum only depends on the low-frequency component of the turbulence and is therefore relatively independent of its spectral shape. This is in contrast to the spectral shape produced by the first term, which is primarily determined by the turbulence spectrum Ψ_o. The second term is expected to underpredict the low-frequency component of the spectrum where the appropriate Green's function is expected to involve more than a single instability wave mode.

Figure 8 is a plot of the spectral shapes computed from (10.4) for the $n = 1$ azimuthal instability mode with $M = 1.5$ (but neglecting the cross-coupling terms) at the polar angles corresponding to the experimental data in figure 7. We have taken $M_c = 0.65M$, $b_2 = 4$, $b_s = (\bar{\omega}_s^6/2)$ and $\bar{\omega}_s = 10$ in all of these calculations. The spread rate is calculated from $\varepsilon = 1.35\,(0.165 - 0.045M^2)/\sqrt{\pi}$ (Lau, Morris & Fisher 1976).

The computed results, which are for a ring source at $\eta' = 0.625$, are seen to exhibit the general characteristics of the data shown in figure 7: namely the spectral peak at $\theta = 30°$ is about a factor of ten larger, and occurs at a lower frequency than that at $\theta = 90°$. Each of the two terms in (10.4) produces a distinct lobe in the small-angle spectrum, with the low-frequency lobe resulting from the second of these. The dip can probably be attributed to our neglect of the interaction terms. Of course, the actual acoustic spectrum produced by the jet is a sum over these individual point contributions and will probably not exhibit distinct lobes – even when the interaction terms are neglected. The summation should also produce a smoother result.

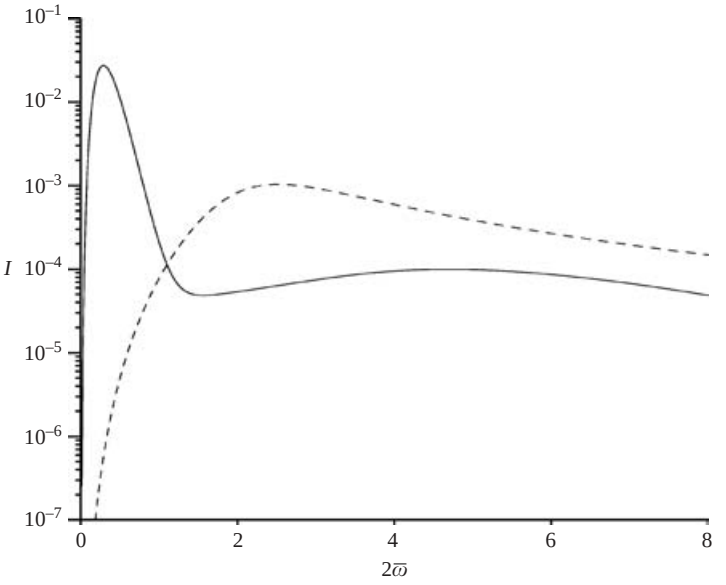

FIGURE 8. Far-field acoustic spectrum computed from equation (9.4). $M = 1.5$; $\theta = 30^\circ$ (solid), $\theta = 90^\circ$ (dashed).

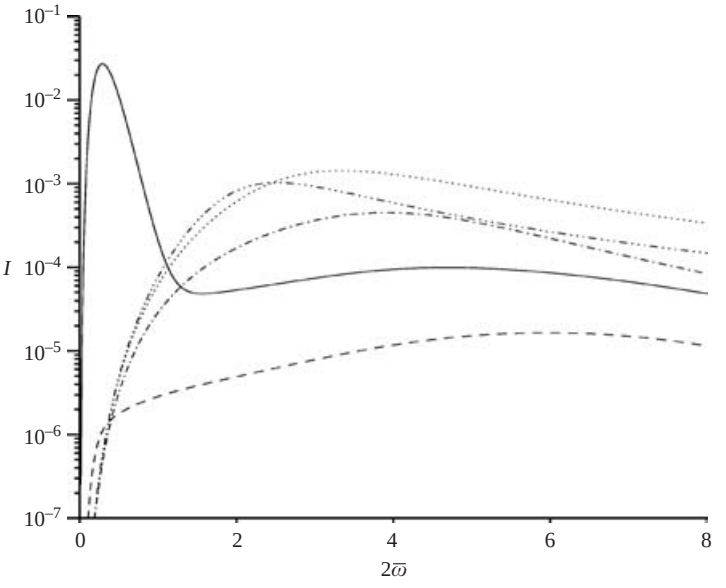

FIGURE 9. Far-field acoustic spectrum computed from equation (9.4). $M = 1.5$; $\theta = 30^\circ$ (solid), $\theta = 40^\circ$ (dashed), $\theta = 60^\circ$ (dash-dot), $\theta = 75^\circ$ (dotted), $\theta = 90^\circ$ (dash-dot-dot).

The $M = 1.5$ spectral shapes shown in figure 8 are plotted at a number of additional polar angles in figure 9. The instability wave contribution (i.e. the second term contribution) to the acoustic spectrum disappears rather abruptly when θ becomes larger than about 30°. Figure 10 shows the spectral shapes for $M = 1.4$. The instability

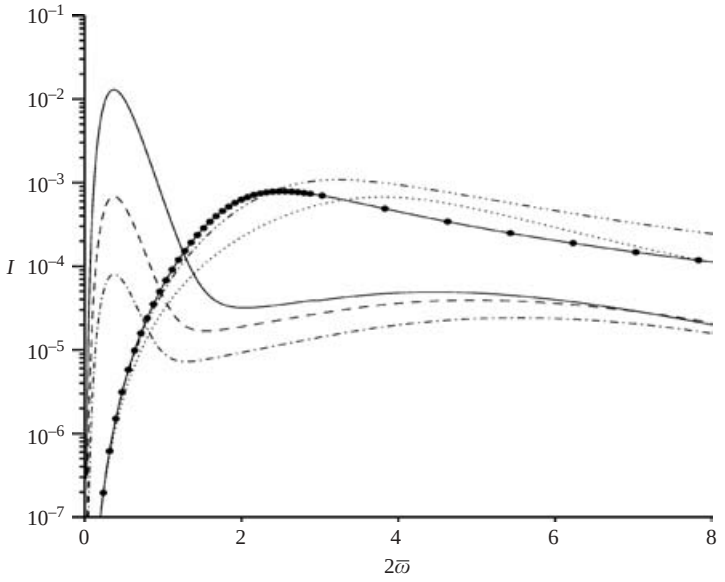

FIGURE 10. Far-field acoustic spectrum computed from equation (9.4). $M = 1.4$; $\theta = 20^\circ$ (solid), $\theta = 25^\circ$ (dashed), $\theta = 30^\circ$ (dash-dot), $\theta = 60^\circ$ (dotted), $\theta = 90^\circ$ (•).

wave contribution at this Mach number maintains the same shape but increases in magnitude as the polar angle decreases.

A major paradox that seems to have eluded explanation is that, while the 90° spectral peaks scale very well with Strouhal number (Gaeta & Ahuja 2003) as predicted by Lighthill's theory, the small-angle spectral peaks observed in high subsonic and low supersonic Mach number experiments scale much better with Helmholtz number (Ahuja 1973; Tam *et al.* 1996). Figure 11 shows that the 90° spectral peak is unchanged while the small-angle spectral peak shifts to lower frequencies as the Mach number increases, which means that the 90° spectrum scales with Strouhal number but that the small-angle spectrum does not. The latter is replotted against the Helmholtz number in figure 12, which shows that the predicted scaling of the spectral peaks is now consistent with experiment.

12. Concluding remarks

The Navier–Stokes equations, rewritten in the form of the linearized Navier–Stokes (LNS) equations with externally applied stress and energy flux sources, which we argue are the natural generalization of the Lighthill (1952) zero-mean-flow acoustic analogy, were solved by using a vector Green's function approach and assuming that the spread rate ε of the mean flow about which the equations are linearized is a small parameter. The relevant solution satisfies causality and the resulting Green's function consists of two components one of which involves spatially growing instability waves. The solution is therefore very different from the parallel flow results even though ε is very small. Numerical results were obtained for a simplified model of a round jet. They show that the small-angle spectrum is narrower and has a lower peak frequency than the 90° spectrum, which is consistent with experimental observations. They also show that while the 90° spectrum scales with Strouhal number as predicted

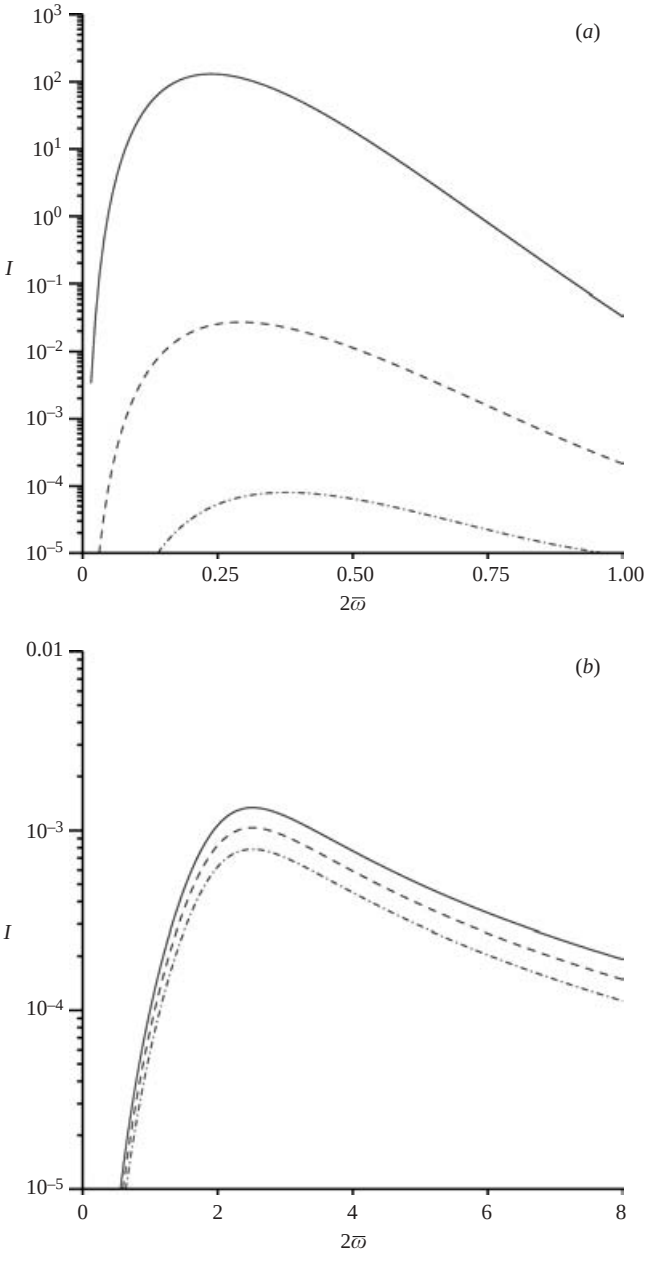

FIGURE 11. Far-field acoustic spectrum vs. Strouhal number, $M = 1.6$ (solid), $M = 1.5$ (dashed), $M = 1.4$ (dash-dot); (*a*) $\theta = 30^\circ$, (*b*) $\theta = 90^\circ$.

by the Lighthill theory, the small-angle spectrum exhibits the experimentally observed Helmholtz number scaling.

Differences in spectral shapes at small and large angles to the jet axis are attributed to the fact that the first component of the Green's function is dominant at $\theta = 90^\circ$ while the second component is dominant at small θ – and not to refraction and the spectral broading resulting from a Doppler frequency shift.

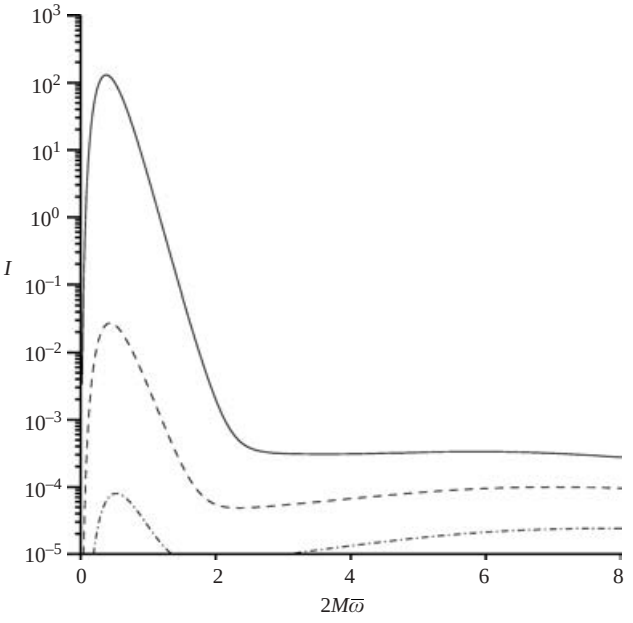

FIGURE 12. Far-field acoustic spectrum vs. Helmholtz number, $\theta = 30°$; $M = 1.6$ (solid), $M = 1.5$ (dashed), $M = 1.4$ (dash-dot).

The authors would like to thank Dr Lennart Hultgren for the use of his Rayleigh equation code, Dr Louis Handler for providing a subroutine used in the spectral computation and Dr Milo Dahl for his comments on the manuscript.

Appendix A

As in (5.1) and (5.2), the mean pressure, density, and Reynolds stresses expand as

$$\bar{p} = P(X, \boldsymbol{x}_\perp) + \varepsilon P^{(1)}(X, \boldsymbol{x}_\perp) + \varepsilon^2 P^{(2)}(X, \boldsymbol{x}_\perp) + \ldots, \tag{A 1}$$

$$\bar{\rho} = \bar{R}(X, \boldsymbol{x}_\perp) + \varepsilon R^{(1)}(X, \boldsymbol{x}_\perp) + \ldots, \tag{A 2}$$

and

$$\tilde{T}_{\mu j} = T^{(0)}_{\mu j} + \varepsilon T^{(1)}_{\mu j} + \varepsilon^2 T^{(2)}_{\mu j} + \ldots, \tag{A 3}$$

with similar expansions for $\tilde{h}$, $\tilde{H}_j$ and $\tilde{H}_o$ implied by equations (2.6) and (3.11). Substituting these into the mean flow equations (2.5) with $\bar{\sigma}_{ij} = \bar{q}_j = 0$, and assuming that the Reynolds stresses vanish in the free stream, shows that the result will only balance if

$$T^{(0)}_{1j} = T^{(0)}_{j1} = T^{(0)}_{4j} = 0 \quad \text{for } j = 2, 3, \tag{A 4}$$

$$\frac{\partial}{\partial x_j}\left(P - T^{(0)}_{jj}\right) = \frac{\partial}{\partial x_l} T^{(0)}_{jl} \quad (\text{no sum on } j \neq l = 2, 3) \tag{A 5}$$

and

$$\frac{\partial}{\partial x_j}\left(P^{(1)} - T^{(1)}_{jj}\right) = \frac{\partial}{\partial x_l} T^{(1)}_{jl} \quad (\text{no sum on } j \neq l = 2, 3). \tag{A 6}$$

The lowest-order mean flow equations become

$$\mathrm{D}_o \bar{R} = 0 \tag{A 7}$$

$$\mathrm{D}_o \bar{R} U = S \tag{A 8}$$

$$\mathrm{D}_o \bar{R} V_j + \frac{\partial P^{(2)}}{\partial x_j} = \frac{\partial}{\partial X} T_{j1}^{(1)} + \frac{\partial T_{jl}^{(2)}}{\partial x_l} \quad \text{for} \quad j, l = 2, 3, \tag{A 9}$$

and

$$\mathrm{D}_o \left(\frac{\gamma}{\gamma - 1} P + \tfrac{1}{2} \bar{R} U^2 \right) = \frac{\partial}{\partial X} \left[T_{41}^{(0)} + U T_{11}^{(0)} + \tfrac{1}{2} U \left(T_{11}^{(0)} + T_{ll}^{(0)} \right) \right] + \frac{\partial}{\partial x_j} \left[T_{4j}^{(1)} + U T_{j1}^{(1)} + V_l T_{jl}^{(0)} + \tfrac{1}{2} V_j \left(T_{11}^{(0)} + T_{ll}^{(0)} \right) \right] \quad \text{for} \quad j, l = 2, 3, \tag{A 10}$$

where the operator D_o is now given by

$$\mathrm{D}_o = \frac{\partial}{\partial X} U + \frac{\partial}{\partial x_j} V_j \quad \text{for } j = 2, 3 \tag{A 11}$$

and we have put

$$S \equiv \frac{\partial}{\partial X} \left(T_{11}^{(0)} - P \right) + \frac{\partial}{\partial x_j} T_{1j}^{(1)} \quad \text{for } j = 2, 3. \tag{A 12}$$

Equations (2.22), (A 1) and (A 3) imply that

$$\tilde{\tau}_{ij} = \delta_{ij} \left(P + \varepsilon P^{(1)} \right) - \left(T_{ij}^{(0)} + \varepsilon T_{ij}^{(1)} \right) + O(\varepsilon^2) \tag{A 13}$$

and it therefore follows from (A 5) and (A 6) that

$$\frac{\partial \tilde{\tau}_{ij}}{\partial x_j} = -\varepsilon \delta_{i1} S + O(\varepsilon^2). \tag{A 14}$$

Appendix B

The first-order perturbation of (5.7) is determined by

$$\mathrm{L}_{\mu\nu}^{(0)} g_{\nu\sigma}^{(1)} = -\mathrm{L}_{\mu\nu}^{(1)} g_{\nu\sigma}^{(0)} \tag{B 1}$$

where the right-hand side is explicitly given by

$$\mathrm{L}_{iv}^{(1)} g_{v\sigma}^{(0)} = \left(\frac{\partial}{\partial X} U + U^{(1)} \frac{\partial}{\partial x_1} + \frac{\partial}{\partial x_j} V_j \right) g_{i\sigma}^{(0)} + \delta_{i1} \frac{\partial}{\partial X} g_{4\sigma}^{(0)} + \delta_{i1} \left(\frac{\partial U^{(1)}}{\partial x_j} g_{j\sigma}^{(0)} + \frac{\partial U}{\partial X} g_{1\sigma}^{(0)} \right) + \frac{\partial V_i}{\partial x_j} g_{j\sigma}^{(0)} + \delta_{i1} \frac{S}{\bar{R}} g_{5\sigma}^{(0)}, \tag{B 2}$$

$$\mathrm{L}_{4v}^{(1)} g_{v\sigma}^{(0)} = \left(\frac{\partial}{\partial X} U + U^{(1)} \frac{\partial}{\partial x_1} + \frac{\partial}{\partial x_j} V_j \right) g_{4\sigma}^{(0)} + \frac{\partial}{\partial x_j} \tilde{c_1^2} g_{j\sigma}^{(0)} + \frac{\partial}{\partial X} \tilde{c_o^2} g_{1\sigma}^{(0)} + (\gamma - 1) \left(\frac{\partial U}{\partial X} + \frac{\partial V_i}{\partial x_i} \right) g_{4\sigma}^{(0)} + (\gamma - 1) \frac{S}{\bar{R}} g_{1\sigma}^{(0)} \tag{B 3}$$

and S is given by (A 12).

Appendix C

We eliminate the velocity-like variable from (B 1) to (B 3) (as was done for the zeroth-order solution) to obtain

$$\mathrm{L}g_{4\sigma}^{(1)} = -\frac{\mathrm{D}_o}{\mathrm{D}t}\frac{\partial}{\partial x_i}\widetilde{c_0^2}\mathrm{L}_{iv}^{(1)}g_{v\sigma}^{(0)} + 2\frac{\partial U}{\partial x_j}\widetilde{c_0^2}\frac{\partial}{\partial x_1}\mathrm{L}_{jv}^{(1)}g_{v\sigma}^{(0)} + (\gamma-1)\frac{\mathrm{D}_o^2}{\mathrm{D}t^2}\mathrm{L}_{4v}^{(1)}g_{v\sigma}^{(0)}. \tag{C 1}$$

This result, together with (5.16), shows that $g_{4\sigma}^{(1)}$ must have a two-term decomposition similar to that of (5.21). The first term remains uniformly small compared to the corresponding term in the zeroth-order solution and need not be considered further. The second must be of the form

$$-2\pi\mathrm{i}\sum_n\int_{-\infty}^{\infty}\frac{\widetilde{c_o^2}(\boldsymbol{x}'_\perp)a_{lj}\varphi_{4nl}^{(1)}(\boldsymbol{x}_\perp)}{[\kappa_n U(\boldsymbol{x}'_\perp)-\omega]^2\Delta'_n(\omega, X')}\mathrm{D}'_\sigma\exp\left(\mathrm{i}\left[\frac{1}{\varepsilon}\int_{X'}^{X}\kappa_n\mathrm{d}X-\omega(t-t')\right]\right)\varphi_{nj}(\boldsymbol{x}'_\perp)\,\mathrm{d}\omega, \tag{C 2}$$

where $\varphi_{4nl}^{(1)}(\boldsymbol{x}_\perp)$ is determined from

$$\mathscr{L}_{\kappa_n}\varphi_{4nl}^{(1)} = -\frac{\partial}{\partial x_j}\frac{\widetilde{c_o^2}}{(\kappa_n U-\omega)^2}\mathrm{L}_{jv}^{(1)}A_{nl}\varphi_{vnl} - \frac{\mathrm{i}\kappa_n\widetilde{c_o^2}}{(\kappa_n U-\omega)^2}\mathrm{L}_{1v}^{(1)}A_{nl}\varphi_{vnl} + \frac{\mathrm{i}(\gamma-1)}{\kappa_n U-\omega}\mathrm{L}_{4v}^{(1)}A_{nl}\varphi_{vnl} \quad \text{(no sum on } n, l) \tag{C 3}$$

and we have assumed, for simplicity, that the higher-order terms in the expansions for the empirically determined stresses $\tilde{T}_{vj}$ have been chosen so that $U^{(1)} = \widetilde{c_1^2} = 0$ in order to make $\mathrm{L}_{v\mu}^{(1)}$ independent of both x_1 and t. We have set

$$\varphi_{4nl} \equiv \varphi_{nl}. \tag{C 4}$$

Comparing (C 1) to (C 4) with (B 2), (B 3), and (5.7) shows that

$$\varphi_{jnl} = \frac{i(\gamma-1)}{(\kappa_n U-\omega)}\frac{\partial\varphi_{nl}}{\partial x_j}, \quad j=2,3, \tag{C 5}$$

$$\varphi_{1nl} = -\frac{(\gamma-1)\kappa_n}{(\kappa_n U-\omega)}\varphi_{nl} - \frac{(\gamma-1)}{(\kappa_n U-\omega)^2}\frac{\partial U}{\partial x_j}\frac{\partial\varphi_{nl}}{\partial x_j} \tag{C 6}$$

and

$$\begin{aligned}\varphi_{5nl} &= \frac{\mathrm{i}}{(\kappa_n U-\omega)}\frac{\partial\varphi_{jnl}}{\partial x_j} - \frac{\kappa_n}{(\kappa_n U-\omega)}\varphi_{1nl}\\ &= -(\gamma-1)\left[\frac{\partial}{\partial x_j}\left(\frac{1}{(\kappa_n U-\omega)^2}\frac{\partial\varphi_{nl}}{\partial x_j}\right) - \frac{\kappa_n^2}{(\kappa_n U-\omega)^2}\varphi_{nl}\right]\\ &= \frac{(\gamma-1)}{\widetilde{c_o^2}}\left[\varphi_{nl} + \frac{1}{(\kappa_n U-\omega)^2}\frac{\partial\varphi_{nl}}{\partial x_j}\frac{\partial\widetilde{c_o^2}}{\partial x_j}\right]\end{aligned} \tag{C 7}$$

with $j=2,3$ and no sum on n.

Since $\mathscr{L}_k$ is self-adjoint and

$$\mathscr{L}_{\kappa_n}\varphi_{nl} = 0 \tag{C 8}$$

by definition, multiplying (C 3) by φ_{nl}, integrating over $\boldsymbol{x}_\perp$ and using the results in Appendix A shows that the left-hand side of this equation must vanish and it follows

that A_{nl} must satisfy (6.3) with

$$(\gamma-1)h_{nl}^{(0)} = \int \frac{\widetilde{c_o^2}U}{(\kappa_n U-\omega)^2}\left(\frac{\partial\varphi_{nl}}{\partial x_j}\varphi_{jnl} - \mathrm{i}\kappa_n\varphi_{nl}\varphi_{1nl}\right)\mathrm{d}\boldsymbol{x}_\perp$$
$$+\mathrm{i}(\gamma-1)\int \frac{1}{(\kappa_n U-\omega)}\left[\left(U-\frac{\kappa_n\widetilde{c_o^2}}{(\kappa_n U-\omega)}\right)\varphi_{nl}^2 + \frac{\widetilde{c_o^2}}{\gamma-1}\varphi_{nl}\varphi_{1nl}\right]\mathrm{d}\boldsymbol{x}_\perp$$
$$= 2\mathrm{i}(\gamma-1)\int \frac{\widetilde{c_o^2}}{(\kappa_n U-\omega)^3}\left(U\frac{\partial\varphi_{nl}}{\partial x_j}\frac{\partial\varphi_{nl}}{\partial x_j} + \omega\kappa_n\varphi_{nl}^2\right)\mathrm{d}\boldsymbol{x}_\perp \qquad (C\,9)$$

where we have used (C 8) and integrated by parts to obtain this result and

$$(\gamma-1)h_{nl}^{(1)} = \int \frac{\widetilde{c_o^2}}{(\kappa_n U-\omega)^2}\left(\frac{\partial\varphi_{nl}}{\partial x_j}\mathrm{L}_{jv}^{(1)}\varphi_{vnl} - \mathrm{i}\kappa_n\varphi_{nl}\mathrm{L}_{iv}^{(1)}\varphi_{vnl}\right)\mathrm{d}\boldsymbol{x}_\perp$$
$$+\mathrm{i}(\gamma-1)\int \frac{\varphi_{nl}}{(\kappa_n U-\omega)}\mathrm{L}_{4v}^{(1)}\varphi_{vnl}\mathrm{d}\boldsymbol{x}_\perp \qquad (C\,10)$$

with $j=2,3$ and no sum on n,l.

Equations (B 2) and (B 3) show that (C 10) can be written as

$$h_{nl}^{(1)} = \int\left[\frac{\widetilde{c_o^2}}{(\kappa_n U-\omega)^2}\left(\frac{\partial\varphi_{nl}}{\partial x_j}d_j + \kappa_n\varphi_{nl}d_1\right) + \frac{\varphi_{nl}}{(\kappa_n U-\omega)}d_4\right]\mathrm{d}\boldsymbol{x}_\perp \qquad (C\,11)$$

where

$$d_1 \equiv \left(\mathrm{D}_o + \frac{\partial U}{\partial X}\right)\hat{\varphi}_{1nl} - \frac{\partial}{\partial X}\varphi_{nl} - \frac{S}{\bar{\rho}\widetilde{c_o^2}}\hat{\varphi}_{5nl}, \qquad (C\,12)$$

$$d_j \equiv \mathrm{D}_o\frac{1}{(\kappa_n U-\omega)}\frac{\partial\varphi_{nl}}{\partial x_j} + \frac{\partial V_j}{\partial x_r}\frac{1}{(\kappa_n U-\omega)}\frac{\partial\varphi_{nl}}{\partial x_r} \qquad (C\,13)$$

and

$$d_4 = \mathrm{D}_o\varphi_{nl} - \frac{\partial}{\partial X}\widetilde{c_o^2}\hat{\varphi}_{1nl} + (\gamma-1)\left(\frac{\partial V}{\partial X} + \frac{\partial V_j}{\partial x_j}\right)\varphi_{nl} - \frac{S}{\bar{\rho}}(\gamma-1)\hat{\varphi}_{1nl}, \qquad (C\,14)$$

where D_o is now given by (A 11), and $\hat{\varphi}_{1nl} \equiv -\varphi_{1nl}/(\gamma-1)$ and $\hat{\varphi}_{5nl} \equiv \widetilde{c_o^2}\varphi_{5nl}/(\gamma-1)$ can be obtained from (C 5) and (C 6).

Appendix D

To evaluate the second term of (6.34), note that $\bar{\alpha}$ must expand like

$$\bar{\alpha} = \xi - \bar{\alpha}_o(\xi)/R_\perp - \bar{\alpha}_1(\xi)/R_\perp^2 + \ldots \quad \text{as } R_\perp \to \infty \qquad (D\,1)$$

where

$$\xi = X/R_\perp = O(1) \qquad (D\,2)$$

when θ and the Mach number M are sufficiently large. Inserting this into (6.19) and (6.20) and expanding the results shows that

$$\bar{\kappa} = \kappa(\bar{\alpha}_o + \bar{\alpha}_1/R_\perp + \ldots) = \kappa(\bar{\alpha}_o) + \kappa'(\bar{\alpha}_o)\,\bar{\alpha}_1/R_\perp + \ldots. \qquad (D\,3)$$

Then inserting this together with (D 1) into (6.21) and expanding that result shows that

$$\xi - \frac{\bar{\alpha}_o}{R_\perp} = \frac{\kappa(\bar{\alpha}_o) + \kappa'(\bar{\alpha}_o)\bar{\alpha}_1/R_\perp + \ldots}{\mathrm{i}\sqrt{\kappa^2(\bar{\alpha}_o) + 2\bar{\alpha}_1\kappa(\bar{\alpha}_o)\kappa'(\bar{\alpha}_o)/R_\perp - (\omega/c_\infty)^2 + \ldots}}$$
$$= \frac{1}{\mathrm{i}\sqrt{\kappa^2(\bar{\alpha}_o) - (\omega/c_\infty)^2}}\left[\kappa(\bar{\alpha}_o) + \left(\kappa'(\bar{\alpha}_o)\bar{\alpha}_1 - \frac{\kappa^2(\bar{\alpha}_o)\kappa'(\bar{\alpha}_o)\bar{\alpha}_1}{\kappa^2(\bar{\alpha}_o) - (\omega/c_\infty)^2}\right)\frac{1}{R_\perp} + \ldots\right]. \tag{D 4}$$

This means that

$$\xi = \frac{\kappa(\bar{\alpha}_o)}{\mathrm{i}\sqrt{\kappa^2(\bar{\alpha}_o) - (\omega/c_\infty)^2}} \tag{D 5}$$

with the choice of branch discussed in connection with (6.10) and

$$\bar{\alpha}_o = \frac{(\omega/c_\infty)^2\kappa'(\bar{\alpha}_o)\bar{\alpha}_1}{\mathrm{i}[\kappa^2(\bar{\alpha}_o) - (\omega/c_\infty)^2]^{3/2}} \tag{D 6}$$

which can be inverted to show that

$$\kappa(\bar{\alpha}_o) = \left(\frac{\omega}{c_\infty}\right)\frac{\xi}{\sqrt{1+\xi^2}}, \tag{D 7}$$

(see (7.4), (7.5), and (D 2)) and

$$\bar{\alpha}_1 = -\left(\frac{\omega}{c_\infty}\right)\frac{\bar{\alpha}_o}{\kappa'(\bar{\alpha}_o)(1+\xi^2)^{3/2}}. \tag{D 8}$$

Inserting these into (D 3) shows that $\bar{\kappa}$ behaves like

$$\bar{\kappa} = \frac{\omega}{c_\infty}\left[\frac{\xi}{\sqrt{1+\xi^2}} + \frac{\bar{\alpha}_o}{R_\perp(1+\xi^2)^{3/2}} + \ldots\right] \quad \text{as } R_\perp \to \infty, \tag{D 9}$$

and inserting this into (6.18) shows that when θ and M are sufficiently large

$$\Theta \to \frac{\omega}{c_\infty}R + \Theta^\infty(\theta, X') + \ldots \quad \text{as } R_\perp \to \infty \tag{D 10}$$

where R is the radial coordinate defined in (7.6) and $\Theta^\infty(\theta, X')$ is defined by (7.10).

Equations (6.21), (D 1), and (D 7) imply that

$$\frac{\mathrm{d}\bar{\alpha}}{\mathrm{d}\bar{\kappa}} = \left(\frac{\omega}{c_\infty}\right)^2\left(\frac{\bar{\alpha}}{\bar{\kappa}}\right)^3 \to \frac{1}{(\omega/c_\infty)\sin^3\theta} \quad \text{as } R \to \infty. \tag{D 11}$$

It follows that

$$\alpha'(X_o) = \frac{\mathrm{d}\bar{\alpha}}{\mathrm{d}\bar{\kappa}}\kappa'(X_o) \to \frac{\kappa'(\bar{\alpha}_o)}{(\omega/c_\infty)\sin^3\theta} \tag{D 12}$$

and therefore that the amplitude factor in (6.30) behaves like

$$\frac{1}{\sqrt{1+\alpha' R_\perp}} \to \frac{(\omega/c_\infty)^{1/2}\sin\theta}{\sqrt{R\kappa'(\bar{\alpha}_o)}} \quad \text{as } R \to \infty. \tag{D 13}$$

Differentiating (7.10) and using (6.19) to (6.21), (D 2), (D 3), and (D 12) shows that

$$\frac{\partial\Theta^\infty}{\partial X'} = -\kappa(X'), \tag{D 14}$$

which means that

$$\frac{\partial}{\partial x_1'}\mathrm{e}^{\mathrm{i}\Theta^\infty/\varepsilon} = D_1'\,\mathrm{e}^{\mathrm{i}\Theta^\infty/\varepsilon} = -\mathrm{i}\kappa\,\mathrm{e}^{\mathrm{i}\Theta^\infty/\varepsilon}. \tag{D 15}$$

Appendix E

Taking the Laplace–Fourier transform of (5.8) yields

$$\frac{(kU-\omega)^2}{\widetilde{c_0^2}}\mathscr{L}_k\bar{G}^{(0)}_{4\sigma} = \frac{(kU-\omega)^2}{\widetilde{c_0^2}}\partial_\sigma\left[\frac{\widetilde{c_0^2}\delta(\boldsymbol{x}_\perp-\boldsymbol{x}'_\perp)}{(kU-\omega)^2(2\pi)^2}\right] + \mathrm{i}\left[k\delta_{\sigma 1}-(\gamma-1)\frac{(kU-\omega)}{\widetilde{c_0^2}}\delta_{\sigma 4}\right]\frac{\delta(\boldsymbol{x}_\perp-\boldsymbol{x}'_\perp)}{(2\pi)^2}, \tag{E 1}$$

where ∂_σ is defined by equation (2.15) and $\mathscr{L}_k$ denotes the Rayleigh operator (5.11). Transferring the derivatives of the δ-function to the source variable $\boldsymbol{x}'$ yields

$$\frac{(kU-\omega)^2}{\widetilde{c_0^2}}\mathscr{L}_k\bar{G}^{(0)}_{4\sigma} = \frac{\widetilde{c_0^2}(\boldsymbol{x}'_\perp)}{(\gamma-1)[kU(\boldsymbol{x}'_\perp)-\omega]^2}\partial'_\sigma\frac{[kU(\boldsymbol{x}'_\perp)-\omega]^2}{\widetilde{c_0^2}(\boldsymbol{x}'_\perp)}\frac{\delta(\boldsymbol{x}_\perp-\boldsymbol{x}'_\perp)}{(2\pi)^2} + \mathrm{i}\left[\frac{k\delta_{\sigma 1}}{\gamma-1}-\frac{(kU-\omega)}{\widetilde{c_0^2}}\delta_{\sigma 4}\right]\frac{\delta(\boldsymbol{x}_\perp-\boldsymbol{x}'_\perp)}{(2\pi)^2} \tag{E 2}$$

where ∂'_σ is given by equation (2.15) but with x_i replaced by x'_i and the dependence on the slow variable X has been suppressed, since it enters only parametrically. It is now clear that the solutions to these equations can all be expressed in terms of the solution $\bar{G}_o(\omega, k, X; \boldsymbol{x}_\perp|\boldsymbol{x}'_\perp)$ of (5.10) by

$$\bar{G}^{(0)}_{41} = \frac{\mathrm{i}k\,\widetilde{c_0^2}(\boldsymbol{x}'_\perp)}{[kU(\boldsymbol{x}'_\perp)-\omega]^2}\bar{G}_o(\boldsymbol{x}_\perp|\boldsymbol{x}'_\perp), \tag{E 3a}$$

$$\bar{G}^{(0)}_{4j} = -\frac{\widetilde{c_0^2}(\boldsymbol{x}'_\perp)}{[kU(\boldsymbol{x}'_\perp)-\omega]^2}\frac{\partial}{\partial x'_j}\bar{G}_o(\boldsymbol{x}_\perp|\boldsymbol{x}'_\perp) \quad \text{for } j=2,3, \tag{E 3b}$$

$$\bar{G}^{(0)}_{44} = -\frac{\mathrm{i}(\gamma-1)}{kU(\boldsymbol{x}'_\perp)-\omega}\bar{G}_o(\boldsymbol{x}_\perp|\boldsymbol{x}'_\perp). \tag{E 3c}$$

REFERENCES

Ahuja, K. K. 1973 Correlation and prediction of jet noise. *J. Sound Vib.* **29**, 155–168.

Avila, G. S. S. & Keller, J. B. 1963 The high frequency asymptotic field of a point source in an inhomogeneous medium. *Commun. Pure Appl. Maths* **XVI**, 363–381.

Balsa, T. F., Gliebe, P. R., Kantola, R. A., Mani, R., Strings, E. J. & Wong, J. C. F. II 1978 High velocity jet noise source location and reduction. *FAA Rep.* FAA-RD-76-79.

Bers, A. 1975 Linear waves and instabilities. In *Plasma Physics* (ed. C. DeWitt & J. Perraud.), pp. 113–2166. Gordon & Beach.

Betchov, R. & Criminale, W. O. 1967 *Stability of Parallel Flows.* Academic.

Briggs, R. J. 1964 *Electron Stream Interaction with Plasmas.* Massachusetts Institute of Technology Press.

Burgers, J. M. 1948 A mathematical model illustrating the theory of turbulence. In *Advances in Applied Mechanics* (ed. R. von Mises & T. von Kármán), pp. 171–199. Academic.

Crighton, D. G. & Gaster, M. 1976 Stability of slowly diverging jet flow. *J. Fluid Mech.* **77**, 397–413.

Carrier, G. F., Krook, M. & Pearson, C. E. 1966 *Functions of a Complex Variable*. McGraw-Hill.

Dowling, A. P., Ffowcs Williams, J. E. & Goldstein, M. E. 1978 Sound propagation in a moving stream. *Phil. Trans. R. Soc. Lond.* A **288**, 321–349.

Favre, A. 1969 Statical equations of turbulent gases. In *Problems of Hydrodynamics and Continuum Mechanics*, SIAM, Philadelphia.

Freund, J. B. 2002 Turbulent jet noise: shear noise, self-noise, and other contributions. *AIAA paper* 2002–2423.

Ffowcs Williams, J. E. 1963 The noise from turbulence converted at high speed. *Phil. Trans. R. Soc. Lond.* A **225**, 469–503.

Goldstein, M. E. 1976 *Aeroacoustics*. McGraw-Hill.

Goldstein, M. E. 2002 A unified approach to some recent developments in jet noise theory. *Intl J. Aeroacoust.* **1**, 1–16.

Goldstein, M. E. & Handler, L. M. 2003 The role of instability waves in predicting jet noise. *AIAA Paper* 2003–3256.

Gaeta, R. J. & Ahuja, K. K. 2003 Subtle differences in jet-noise scaling with narrowband spectra compared to 1/3 octave band. *AIAA Paper* 2003–3124.

Khavaran, A. & Bridges, J. 2004 Modelling of turbulence generated noise in jets. *AIAA Paper* 04-2983.

Lau, J. C., Morris, P. J. & Fisher, M. J. 1976 Turbulence measurements in subsonic and supersonic jets using a laser velocimeter. *AIAA Paper* 76–348.

Lighthill, M. J. 1952 On sound generated aerodynamically: I. General theory. *Proc. R. Soc. Lond.* A **211**, 564–587.

Lighthill, M. J. 1954 On sound generated aerodynamically: II. Turbulence as a source of sound. *Proc. R. Soc. Lond.* A **222**, 1–32.

Lilley, G. M. 1974 On the noise from jets. *Noise Mechanism*, AGARD–CP–131, pp. 13.1–13.12.

Mani, R. 1976 Influence of jet flow on jet noise. *J. Fluid Mech.* **173**, 753–793.

Morse, P. M. & Feshbach, H. 1953 *Methods of Theoretical Physics*. McGraw-Hill.

Norum, T. 1994 NASA-Langley Jet Noise Lab Generic Nozzle Narrow Band Spectra, vol. 1 (unpublished, available electronically).

Phillips, O. M. 1960 On the generation of sound by supersonic turbulent shear layers. *J. Fluid Mech.* **9**, 1–28.

Pierce, A. D. 1981 *Acoustics: An Introduction to its Physical Principles and Applications*. McGraw-Hill.

Pope, S. B. 2000 *Turbulent Flows*. Cambridge University Press.

Pridmore-Brown, D. C. 1958 Sound propagation in a fluid flowing through an attenuating duct. *J. Fluid Mech.* **4**, 393–406.

Speziale, C. G. 1991 Analytical methods for the development of Reynolds-stress closure in turbulence. *Annu. Rev. Fluid Mech.* **23**, 107–157.

Speziale, C. G. & So, M. C. 1998 Turbulence modeling a simulation. In *Handbook of Fluid Dynamics* (ed. R. Johnson), CRC Press.

Tam, C. K. W. 1995 Supersonic jet noise. *Annu. Rev. Fluid Mech.* **27**, 17–44.

Tam, C. K. W. & Morris, P. J. 1980 The radiation of sound by instability waves of a compressible plane turbulent mixing layer. *J. Fluid Mech.* **98**, 349–381.

Tam, C. K. W. & Burton, D. E. 1984 Sound generated by instability waves of supersonic flows. Parts 1 and 2. *J. Fluid Mech.* **138**, 249–295.

Tam, C. K. W., Golebiowski, M. & Seiner, J. M. 1996 On the two components of turbulent mixing noise from supersonic jets. *AIAA Paper*. 96–1716.

Van Dyke, M. 1975 *Perturbation Methods in Fluid Mechanics*. The Parabolic Press.

Wundrow, D. W. 1996 Linear instability of a uni-directional transversely sheared mean flow. *NASA CR*–1985.